Title: Rapid ethylene-triggered protein complex remodeling in dark grown hypocotyls

Keywords: Arabidopsis, hypocotyl, ethylene, triple responses, EIN2, protein complex dynamics, CFMS, quantitative proteomics, protein localization

Authors

Youngwoo Lee[1,2,‡], Hye Lin Park[1,2,‡], Gyeong Mee Yoon[1,2,*], Daniel B Szymanski[1,3,*]

Affiliations

[1]Department of Botany and Plant Pathology, Purdue University, West Lafayette, IN, USA

[2]Center for Plant Biology, Purdue University, West Lafayette, IN, USA

[3]Department of Biological Sciences, Purdue University, West Lafayette, IN, USA

*Correspondence to: dszyman@purdue.edu and yoong@purdue.edu

[‡] These authors contributed equally to this work.

Abstract

Protein-level cellular dynamics, including multimerization, play a crucial role in rapid adaptation of plants during developmental transitions and environmental stresses. The gaseous hormone ethylene is a key regulator of these rapid cellular adjustments, especially in growth inhibition. During soil emergence, etiolated seedlings undergo crucial morphological changes to their apical hooks and hypocotyls, with ethylene inhibiting hypocotyl axial elongation while promoting radial expansion. Ethylene triggers these growth responses within two hours; however, the protein machineries and cellular processes that mediate morphogenesis control are not known. Here, we used quantitative proteomics and co-fractionation mass spectrometry to test for rapid ethylene-dependent changes in protein abundance and protein complex composition. Protein multimerization responses were numerous and diverse. There were instances of protein complex assembly and disassembly, with varying degrees of completeness. Small-scale validation tests indicate that the identified proteins play a role in hypocotyl development and suggest that this novel approach to gene discovery identifies potential targets for ethylene-mediated growth regulation and enhanced seedling adaptability during early development.

Introduction

Among many ethylene-regulated developmental processes (Abeles et al., 1992; Bleecker and Kende, 2000; Alonso and Ecker, 2001), ethylene modulation of hypocotyl development in darkness is a classic example of hormone-regulated developmental plasticity. It is thought that ethylene levels increase as the subterranean seedling encounters stiff physical barriers, and this leads to an altered growth habit that increases the likelihood of soil emergence (Von Arnim and Deng, 1996; Smalle et al., 1997). In dark-grown seedlings, ethylene induces biphasic hypocotyl growth inhibition (Phase I and II), with distinct mechanisms governing each phase over a two-hour timeline (Binder et al., 2004; Binder, 2007). Phase I begins rapidly, within 10-15 minutes of ethylene exposure, reducing the growth rate by ~50 %. This initial suppression is mediated non-transcriptionally via Ethylene-insensitive 2 (EIN2), a positive regulator of ethylene signaling, which modulates cellular processes like microtubule stabilization and cell wall remodeling (Binder et al., 2004). Phase II follows as a sustained inhibition that initiates about 30 minutes after ethylene exposure. It requires the transcription factors EIN3/EIN3-like (EIL), which activate genes such as WAVE-DAMPENED-LIKE 5 (WDL5) to further suppress growth by enhancing microtubule stability (Sun et al., 2015). Ethylene primarily targets the epidermal cells of the hypocotyl (Smalle et al., 1997; Vandenbussche et al., 2007; Vandenbussche et al., 2012; Das et al., 2016; Seo and Yoon, 2019), where it suppresses elongation by disrupting cortical microtubule arrays and promoting microtubule stabilization, thus enforcing cell growth inhibition. Within two hours, growth is profoundly inhibited but not entirely halted, maintaining this low growth baseline. Despite this detailed characterization of the biphasic response in hypocotyl growth inhibition, the dynamic molecular mechanism governing protein abundance changes and complex formation such as multimerization during ethylene-mediated hypocotyl growth suppression remains poorly understood.

Ethylene signaling operates through several well-characterized signal transduction. Upon binding to ethylene receptors at the ER, ethylene inactivates the receptors, releasing their inhibition of Ethylene-insensitive 2 (EIN2), which subsequently activates EIN3/EIN3-like (EIL) transcription factors. This triggers the expression of Ethylene Response Factor (ERF) transcription factors that regulate genes involved in growth suppression (Ju et al., 2012; Qiao et al., 2012; Wen et al., 2012). The downstream targets of ethylene that mediate growth modulation are not well characterized. At the cellular level, ethylene may inhibit axial cell elongation by reducing cell wall extensibility through altered transcription of several proteins including expansins, xyloglucan endotransglucosylase/hydrolases (XTHs), and peroxidases (Van de Poel et al., 2015; Qin et al., 2019). Ethylene also modifies microtubule organization, which affects cellulose deposition patterns in the cell wall that could affect axial expansion (Van de Poel et al., 2015). Furthermore, ethylene exerts its negative impact on plant growth through crosstalk with other phytohormones. Ethylene enhances auxin activity through multiple mechanisms, upregulating PIN proteins and AUX1 to promote auxin transport and stimulating auxin biosynthesis (Ruzicka et al., 2007; Swarup et al., 2007; Liu et al., 2018), while simultaneously antagonizing gibberellin (GA) signaling by promoting DELLA protein accumulation and inducing GA catabolism via GA2ox (Achard et al., 2003; Schomburg et al., 2003; Yoo et al., 2009). The interaction with abscisic acid (ABA) adds another layer of complexity but is highly dependent on light conditions and involves complex hormonal crosstalk. In darkness, ABA has little to no effect on hypocotyl growth unless light signaling pathways are constitutively active, as in mutants like *cop1-4* or *pifq*, where ABA can then exert inhibitory effects via auxin transport and the upregulation of DELLA proteins that suppress GA signaling (Ghassemian et al., 2000; Liang et al., 2012; Peng et al., 2022). In contrast, in the presence of light, ethylene promotes

hypocotyl elongation by facilitating COP1-mediated degradation of HY5 and activating PIF3-dependent auxin pathways (Yu et al., 2013).

Modern protein mass spectrometry offers a powerful systems-level approach for understanding proteome response to developmental, physiological, and environmental stimuli (Gingras et al., 2007; Nilsson et al., 2010; Aebersold and Mann, 2016; Lee et al., 2025). In ethylene signaling, proteomics has captured changes in protein abundance, localization, and post-translational modifications (PTMs). Gel-based proteomics (Prayitno et al., 2006; Zheng et al., 2013; Wang et al., 2015; Kim et al., 2018; Shin et al., 2020), stable and isobaric isotope labeling (Wang et al., 2015; Zhang et al., 2015; Du et al., 2016), and phosphoproteomics (Chen et al., 2011; Wang et al., 2015; Zhang et al., 2015), have been applied across plant species to characterize ethylene-responsive proteins and regulatory signaling networks. In climacteric fruits such as apples, kiwifruits, and bananas, ethylene treatment induces proteins involved in hormone biosynthesis, redox regulation, energy metabolism, and defense mechanisms (Zheng et al., 2013; Li et al., 2015; Du et al., 2016; Shin et al., 2020). In banana fruit, pretreatment with ethylene may enhance chilling and heat tolerance by upregulating proteins associated with ATP production, ROS scavenging, and protein turnover (Li et al., 2015; Du et al., 2016). In Arabidopsis, ethylene affects proteins involved in vesicle trafficking, oxidative stress, and hormone crosstalk, while repressing ribosomal proteins and brassinosteroid-regulated proteins (Chen et al., 2011). Further phosphoproteomic studies using *ein2* mutants revealed that ethylene signaling induces a general reduction in phosphorylation levels, with distinct motifs present in both ethylene-enhanced and -repressed phosphopeptides (Chen et al., 2011). Collectively, these studies underscore the versatility of ethylene signaling and highlight the critical roles of translational and post-translational regulation, including phosphorylation motifs and kinase activity, in orchestrating rapid and context-dependent proteomic responses.

Co-fractionation mass spectrometry (CFMS), a strategy that couples biochemical fractionation with mass spectrometry, enables the characterization of endogenous protein complex sizes (Kristensen et al., 2012) and organelle localizations (Andersen et al., 2003) without requiring transgenes or targeted enrichment. CFMS has been extensively utilized to determine the apparent masses and localization of protein complexes in diverse Arabidopsis tissues, including leaves (Aryal et al., 2014; Aryal et al., 2017; McBride et al., 2017) and roots (Gilbert and Schulze, 2019), as well as in organelles such as chloroplasts (Olinares et al., 2010) and mitochondria (Klodmann et al., 2010; Senkler et al., 2017). This approach has enabled the identification and characterization of numerous known and novel protein complexes with compositions across plant species (McBride et al., 2019; McWhite et al., 2020; Lee et al., 2021; Yang et al., 2024; Lee et al., 2025), and has been successfully used to monitor multimerization dynamics during diurnal cycles (Gorka et al., 2019), protein-ligand interactions (Veyel et al., 2017), and over evolutionary timescales (Lee and Szymanski, 2021). However, protein multimerization changes in response to plant hormone signaling have remained largely unexplored.

In this study, we performed proteomic analyses to analyze the protein-level responses underlying the short-term response of growth inhibition induced by ethylene treatment. By leveraging the etiolated hypocotyl growth inhibition system and careful dissection of the target organ, we analyzed the overall proteome-wide ethylene responses in both crude soluble and microsome-associated cellular fractions. Using CFMS and high-throughput statistical analyses, we profiled changes in protein multimerization states following ethylene exposure. Our data revealed proteins showing alterations in abundance, localization, and multimerization, many of which are associated with core cellular functions such as translation, vesicle trafficking, energy metabolism, and hormone-hormone signaling crosstalk. Notably, we observed a lack of correlation between ethylene-induced transcriptional changes and protein

abundance alterations, highlighting the importance of translational and post-translational regulation, as well as protein-protein interactions, in ethylene-mediated growth inhibition. This work provides the first global view of ethylene-dependent multimerization variants and uncovers potential mechanisms of post-translational control during early hormone signaling. Together, our findings demonstrate the power of CFMS to uncover dynamic changes in protein complex assembly and offer a systems-level framework for dissecting ethylene signaling in plants.

Results

Exogenous ethylene inhibits hypocotyl cell growth

To recapitulate ethylene-mediated growth inhibition in response to ethylene exposure, we measured hypocotyl length of three-day-old, etiolated Arabidopsis seedlings exposed to ethylene for two hours (Figure 1A and B). Wild-type Col-0 seedlings showed significant hypocotyl growth inhibition and increased *Ethylene Response Factor 1* (*ERF1*) expression (Figure 1C), while ethylene-insensitive *ein2-5* mutant remained unresponsive (Figure 1B). Consistent with this, at the cellular level, ethylene treatment suppressed the elongation of cells below the cotyledon-hypocotyl junction in wild-type but not in *ein2-5* seedlings (Figure 1D and 1E). These cells typically cover the apical hook and double in length within a day in the dark in wild-type seedlings (Gendreau et al., 1997). Our results demonstrated that two hours of ethylene treatment were sufficient to inhibit hypocotyl elongation. We employed this ethylene treatment condition for subsequent quantitative proteomic analyses.

Identification of soluble and membrane-associated proteins in etiolated hypocotyls

To analyze proteome-wide responses to ethylene during Arabidopsis seedling growth, we dissected hypocotyls from three-day-old, etiolated Col-0 and *ein2-5* mutant seedlings grown in the dark. For our quantitative analysis of protein abundance and crude subcellular localization, hypocotyls were fractionated by differential centrifugation into crude soluble (S200) and microsome-associated (P200) fractions (Figure 2A). The S200 contains soluble proteins from the apoplast, cytosol, and those from broken plastids (Aryal et al., 2014; McBride et al., 2019). The washed P200 fraction is highly enriched in true membrane-associated proteins (McBride et al., 2017). At a 1 % false discovery rate (FDR), 2,146 S200 and 1,079 P200 proteins were reliably detected in at least two out of three biological replicates (Supplemental Datasets S1, S2A, and S3A). We applied a label-free quantification (LFQ) normalization across all samples and defined reproducible proteins as those quantified in at least two out of three replicates. This filtering yielded 1,839 and 865 reproducible proteins from the S200 and P200 fractions, respectively, which were used for downstream analyses (Figure 2B and 2C; Supplemental Datasets S2B and S3B). The reproducibility among replicates and between treatments was high based on Pearson correlation coefficient (PCC) and hierarchical clustering analysis (Supplemental figure S1A and S1B). The third replicate of Col-0 +C_2H_4 S200 exhibited the lowest coverage and clustered separately due to a high number of missing values. Principal component analysis (PCA) clearly resolved genotypes, but the ethylene-treated groups were not resolved from controls, suggesting that ethylene does not have a clear global effect on protein abundance. (Supplemental figure S1C).

The breadth of metabolic pathways associated with the dataset was visualized by mapping the proteome of untreated dark-grown hypocotyls (Col-0 -C_2H_4 S200) onto the Plant Metabolic Network (Supplemental figure S2). This metabolic map underscores that the dark-grown hypocotyl acts as metabolically active tissue, coordinating nitrogen assimilation (e.g., GS/GOGAT cycle), redox homeostasis (e.g., glutathione and thioredoxin systems), and amino acid metabolism (e.g., glutamate,

aspartate, and branched-chain amino acids) to support rapid cell elongation (Bellegarde et al., 2019; Zayed et al., 2023; Zhu et al., 2025). The proteomics data are also consistent with catabolic reactions associated with mobilizing protein and lipids to enable new cell wall and membrane biogenesis (Kim et al., 2013; Fan et al., 2019; Xu and Fan, 2022). Gluconeogenesis, in particular, is essential for the seed-to-seedling transition, as it converts storage lipids into carbon and energy required for early development (Eastmond et al., 2015). The most highly abundant enzymes in the dataset map to central carbon metabolism (Supplemental figure S3), and this presence of highly abundant pyruvate orthophosphate dikinase and pyruvate carboxykinase (Supplemental Dataset S1E) may reflect gluconeogenesis in cytosol. Our data provide a resource to analyze how ethylene modulates protein abundance in pathways associated with energy homeostasis and resource allocation in developing hypocotyls.

Next, we performed two-sample *t*-tests independently for each genotype and compared the statistical results to identify proteins that differed in response to ethylene treatment in Col-0 samples but not in *ein2-5* samples (Supplemental Datasets S2B and S3B). This analysis revealed 16 S200 proteins with at least 4-fold (or ± 2 log2 ratio of $-C_2H_4$ to $+C_2H_4$) abundance changes in response to ethylene in an EIN2-dependent manner (Figure 2D; Supplemental figure S1D). The 14 proteins exhibited reduced levels in the presence of ethylene, including extrinsic subunits of photosystem I and II. Additionally, AtPPC3 (AT3G14940.1) and LTP1 (AT2G38540.1) exhibited significant decreases after ethylene treatment. *AtPPC3* encodes a phosphoenolpyruvate carboxylase (PEPC) involved in oxaloacetate formation and is rapidly induced by nitrate treatment in roots (Vidal et al., 2013). In contrast, the abundance levels of β-galactosidase 15 (BGAL15; AT1G31740.1) and seed storage albumin 4 (SESA4; AT4G27170.1) were significantly increased following ethylene treatment. BGALs hydrolyze β-D-galactosides and are involved in flower senescence and fruit ripening (Ahn et al., 2007; Chandrasekar and van der Hoorn, 2016), and have been shown to regulate their own transcript levels during ripening (Alexander and Grierson, 2002; Moctezuma et al., 2003). SESA4 is important for nitrogen and sulfur provision during germination, and its transcript abundance decreases after brassinolide treatment in Arabidopsis seedlings (Goda et al., 2004). In contrast to the S200 dataset, *t*-tests within the P200 dataset did not reveal any proteins with significant ethylene-dependent changes exceeding the 4-fold difference (Supplemental figure S1D; Supplemental Dataset S3B).

To determine if observed protein level changes in response to ethylene were correlated with transcriptional alteration, we selected 21 high confidence proteins hits from the S200 dataset based on their abundance and spectral counts (Supplemental Dataset S2C) and examined the transcript levels of the corresponding genes (Figure 2E). Seedling growth in darkness for three days with or without ethylene treatment was subjected to qPCR-based gene expression analysis. Unlike *ERF1* control, which showed an 8-fold increase in its transcript in response to ethylene, most of the selected genes showed no transcript changes, while a small subset exhibited concurrent changes at both transcript and protein abundance. ACC oxidase 1 (ACO1; AT2G19590.1) and an amino acid kinase family protein (PUMPKIN; AT3G18680.1), both putatively up-regulated in response to ethylene at the protein level, exhibited corresponding up-regulation at the transcript level. Conversely, the disease resistance-responsive (dirigent-like protein) family protein (DIR; AT4G11210.1), predicted as down-regulated in proteome data (Supplemental Dataset S2C), showed consistent down-regulated at the transcription level. These results suggest that ethylene predominantly regulates protein abundance through post-transcriptional mechanisms rather than transcriptional control during rapid hypocotyl growth inhibition.

Multimerization changes in response to ethylene

To test for protein multimerization changes in response to exogenous ethylene treatment, we performed co-fractionation mass spectrometry (CFMS) on S200 fractions obtained from three-day-old, etiolated Col-0 hypocotyls, either treated with ethylene ($SEC_{Ethylene}$) or left untreated ($SEC_{Untreated}$) (Supplemental figure S4). Biological duplicates of SEC profiles are sufficient to gain reliable information on protein multimerization states (Aryal et al., 2014; Aryal et al., 2017; Gilbert and Schulze, 2019; McBride et al., 2019; Pang et al., 2020; Lee et al., 2021; Lee and Szymanski, 2021; Skinnider and Foster, 2021; Schlossarek et al., 2023). The vast majority of proteins identified in the $SEC_{Untreated}$ and $SEC_{Ethylene}$ samples were detected in both replicates, 2,908 and 2,692, respectively (Figure 3A and 3B; Supplemental Dataset S4). The replicate profiles demonstrated high reproducibility based on PCC values, which were maximal along the diagonal corresponding to identical column fractions in the replicates (Figure 3C and 3D). Most proteins had identical peak locations in the replicates, and approximately 95 % had peaks within a two-fraction shift between replicates for both $SEC_{Untreated}$ and $SEC_{Ethylene}$ (Figure 3E and 3F). Based on this two-fraction reproducibility threshold, we selected 2,796 $SEC_{Untreated}$ proteins and 2,606 $SEC_{Ethylene}$ proteins as reproducible for downstream analyses. To deconvolve proteins with multiple elution peaks, we applied a Gaussian peak detection algorithm (McBride et al., 2017). Reproducible proteins with multiple peaks were assigned with suffixes indicating peak numbers and are included in Supplemental Dataset S5A and S5B. When comparing apparent mass (M_{app}) values to predicted monomeric mass (M_{mono}) values of peaks, the distributions of points on both plots were skewed toward multimeric forms (Figure 2G and 2H), consistent with previous estimates for soluble proteins across various plant species and tissue types (Aryal et al., 2014; McBride et al., 2017; McBride et al., 2019; Lee et al., 2021; Lee and Szymanski, 2021; Lee et al., 2025). These results suggest that ethylene treatment does not induce global changes in protein multimerization. From both datasets, 2,368 proteins were reliably detected in both untreated control and ethylene-treated samples, while 428 and 238 proteins belong only to $SEC_{Untreated}$ and $SEC_{Ethylene}$, respectively (Figure 3I).

To test for instances of ethylene-dependent changes in protein multimerization, we followed published methods (Lee and Szymanski, 2021) to conduct statistical tests of the M_{app} values for the 2,368 proteins (Figure 3I; Supplemental Data S6A). *ANOVA* tests were performed using a 5 % FDR threshold. Proteins flagged by this analysis were further filtered to remove potential false positives. Specifically, raw elution profiles were manually inspected to rule out cases where a minor or clearly co-eluting peak appeared in only one of the replicates. In addition, we excluded less reliable cases in which flagged peaks had similar locations within two column fractions. After filtering, 43 multimerization variants in response to ethylene were predicted (Supplemental Data S6B). Gene Ontology (GO) enrichment analysis at a 1 % false discovery rate (FDR) revealed “structural constituent of ribosome” and “response to cytokinin” as the most significantly enriched molecular function and biological process terms, respectively, among the ethylene-induced multimerization variants (Supplemental Data S7). Notably, eight ribosomal proteins showed altered multimerization states following ethylene treatment, suggesting that ribosomal protein complexes may be remodeled or that their assembly is dynamically regulated in response to ethylene signaling. These changes may be mediated by phosphorylation or other PTMs of ribosomal proteins or associated factors, potentially affecting ribosome biogenesis and function. These findings highlight that ethylene signaling extends beyond transcriptional regulation to influence translational control and ribosome assembly. Six other multimerization variants were associated with the “response to cytokinin” category, including Binding Partner of ACD11 1 (BPA1; AT5G16840.3) and Photosystem II Stability/Assembly Factor (HCF136; AT5G23120.1). BPA1 exhibited a shift from a monomeric peak with an apparent molecular mass of 31 kDa (R_{app} of 1.1) to a multimeric form with a M_{app} of 54.2 kDa

(R_{app} of 2.0) following ethylene treatment, suggesting dimerization. BPA1 is a key regulator of reactive oxygen species (ROS)-mediated defense responses in plants (Li et al., 2019). Its dimeric form may reflect interaction with ACD11, potentially contributing to complex stabilization and proper regulation of programmed cell death. Conversely, HCF136 shifted from a dimeric form (R_{app} of 1.7) to a monomeric or proteolyzed form with a M_{app} of 27.1 kDa (R_{app} of 0.6) after ethylene exposure. HCF136 is essential for the stability and assembly of Photosystem II and selectively regulates PSII biogenesis, particularly under low-light conditions (Plücken et al., 2002). The observed decrease in abundance of PSII complex subunits (Figure 2D) may be associated with HCF136 degradation or disassembly under ethylene treatment. A summary of 26 multimerization variants identified at a stringent FDR (1 %) is provided in Table 1.

We further classified the different types of multimerization behavior based on changes in apparent protein size and the partitioning of the protein pool between distinct forms, as indicated by multiple peaks in the SEC profiles (Table 1). In some instances, ethylene promoted conversion to a more highly assembled state with an increased apparent mass (classified as A or IA in Table 1). For example, the predicted CUL4 E3 ligase substrate receptor DWA1 (AT2G19430.1) assembled into two high-mass forms that were not present in the control (A). In other cases, such as the tubulin folding cofactor complex subunit KIESEL (AT2G30410.2), the increase in assembly was incomplete (IA) because in the presence of ethylene the protein pool was partitioned between a distinct high-mass complex and a lower-mass complex that was also observed in the control. In contrast, ethylene also appeared to cause disassembly or rearrangement of protein from a higher-mass complex to a resolvable lower-mass form. This behavior was classified as disassembly (D) if the lower-mass form was consistent with the monomeric state, e.g., $R_{app} < 1.6$ as in GRBP4 (AT3G23830.2), or having a lower-mass peak matching a peak present in the control TCP-1 (AT3G02530.1). The dynamic was classified as disassembly/reassigned binding partner (D/R) if the lower-mass form was predicted to be multimeric, e.g., $R_{app} > 1.6$, and was unique to the ethylene-treated sample. The distinction is that the lower-mass complex could reflect partial disassembly or the repartitioning of the protein to a novel set of interactors. These R_{app} cut-offs are not foolproof metrics but use known information to predict the simplest explanations that underly protein complex remodeling. D/R rearrangements were classified as incomplete (ID and ID/R) when the higher-mass peak persisted in the ethylene-treated samples, e.g. RPT6A (AT5G19990.1) and RPS11 (ATCG00750.1), respectively.

Detailed analysis of selected ethylene-induced multimerization variants

We focused on a subset of interesting hits for deeper proteomic analyses and gene knockout experiments. DWD (DDB1-binding WD40 protein) hypersensitive to ABA 1 (DWA1 or THO6; AT2G19430.1) had a likely monomeric peak corresponding with a M_{app} of 30 kDa (R_{app} of 0.7) in both $SEC_{Untreated}$ or $SEC_{Ethylene}$ datasets (Figure 4A). Upon ethylene treatment, DWA1 displayed two additional higher mass peaks at 700 kDa (R_{app} of 17.4) and 200 kDa (R_{app} of 5.0), suggesting a transition to multimeric forms. Similarly, Aspartic proteinase A1 (APA1; AT1G11910.1) transitioned from a monomeric state (R_{app} of ~0.7) to a higher-mass complex with a R_{app} of ~12.1 in response to ethylene (Figure 4B). This enzyme is active as a monomer and contains a plant-specific insert (PSI) domain, which can influence enzymatic activity and protein interactions (Mazorra-Manzano et al., 2010). The PSI domain may mediate higher-order complexes with distinct (altered or reduced specificity) activity in response to ethylene signaling.

Interestingly, ATP-binding cassette (ABC) transporter B family member 5 (ABCB5 or P-glycoprotein 5; AT4G01830.1) was classified as a potentially ethylene-induced protein complex since it

was only detected after ethylene treatment (Figure 4C). ABCB5 exhibited multiple peaks with R_{app} values of 2.8 and 0.7 following ethylene treatment. The presence of ABC transporters in S200 proteomic experiments has long been somewhat of a mystery (Aryal et al., 2014; McBride et al., 2019). ABCB5 is a member of the broadly diversified plant ABC transporter family, which mediates the transport of various molecules, including auxin, across biological membranes (Sánchez-Fernández et al., 2001; Verrier et al., 2008). The ABCB transporters, including ABCB5, consist of four domains, two integral transmembrane domains (TMDs), each with six transmembrane helices, and two cytoplasmic nucleotide-binding domains (NBDs), arranged in the order TMD1-NBD1-TMD2-NBD2 (Figure 4D). In this study, three distinct ABCB5 peptides were identified, with two peptides located in NBD1 and one in NBD2. Peptides in NBD1 showed R_{app} values ranging from 0.6 to 0.8, while the peptide in NBD2 displayed R_{app} values between 2.6 and 3.0 (Figure 4E), suggesting proteolysis of the NBD1 and NBD2 regions in response to ethylene treatment. Peptides from two other ABC transporters, ABCB18 and ABCC5, identified in this study also had R_{app} values of 0.6 to 0.8 and were all mapped to NBD1 sequences. Taken together, the proteolyzed NBD2 of ABCB5 may form a distinct protein complex in the cytoplasm during the ethylene response.

To test for a potential link between multimerization variability and hypocotyl development, we examined ethylene-dependent hypocotyl growth responses in *dwa1*, *apa1*, and *abcb5* single loss-of-function mutants (Figure 4F and G). The *dwa1* and *apa1* mutants showed comparable hypocotyl length to wild type when grown without ACC but exhibited reduced ethylene sensitivity with significantly longer hypocotyls when treated with higher ACC concentrations (Figure 4G). The *abcb5* mutant exhibited significantly longer hypocotyls compared to the wild type at various ACC concentrations but uniquely showed enhanced hypocotyl elongation without ethylene treatment (Figure F). Importantly, the proportional reduction in hypocotyl length in response to ethylene remained comparable between WT and *abcb5* mutants (Supplemental figure S5), suggesting that the longer hypocotyl phenotype may not be directly linked to ethylene sensitivity. These results suggest that DWA1 and APA1 contribute to ethylene-mediated hypocotyl growth regulation, whereas ABCB5 appears to have a broader function in modulating general hypocotyl development pathways, potentially including those regulated by auxin.

Discussion

The analysis focused on the proteomic response of dissected hypocotyls after the seedlings were exposed to 100 ppm ethylene for 2 hours. A significant EIN2 and EIN3/EIL-dependent reduction in axial elongation was detectable in this time frame (Figure 1). The proteomic responses of dissected hypocotyls were analyzed following combinations of crude cell fractionation, SEC, an array of label-free quantitative proteomic, and statistical tests for proteins with altered properties in response to short-term ethylene treatment. Of the thousands of proteins in the soluble (S200) and crude microsomal (P200) proteins, only a small subset in the soluble displayed significant changes in abundance (Figure 2D; Supplemental Datasets S2 and S3) or multimerization (Figure 3; Supplemental Dataset S6). Collectively they provide a systems-level view of the multimerization response.

Changes in protein complex composition are expected as they are frequently observed in the early steps of hormone-mediated signal transduction (Zeng et al., 2018). Post-translational modification, particularly phosphorylation, alters protein conformation and interaction capacity by introducing charge-mediated effects, inducing structural changes, or triggering allosteric signaling (Groban et al., 2006; Schonichen et al., 2013). These modifications can either stabilize or destabilize complexes depending on context, enabling precise control over signal transduction and stress responses. Protein cleavage serves as

another critical mechanism by which it dismantles existing complexes or produces active protein fragments that initiate new functions (Berry et al., 2021; Zanotti et al., 2022). Additionally, subcellular redistribution redirects proteins to different cellular compartments, fundamentally changing their potential interaction partners (Park et al., 2023; Chien et al., 2024; Chien and Yoon, 2024; Park and Yoon, 2025).

The global multimerization response to plant hormone treatment has not been previously published. Here we detected a diverse set of proteins with different types of multimerization changes. These changes are most likely to reflect non-covalent, reversible protein-protein interactions that are modulated during short-term ethylene treatment. The chromatographic and protein quantification methods are robust and have been used to quantify multimerization from a broad range of species and sample types (Andersen et al., 2003; Kristensen et al., 2012; Aryal et al., 2014; Aryal et al., 2017; McBride et al., 2017; Gilbert and Schulze, 2019; Gorka et al., 2019; McBride et al., 2019; McWhite et al., 2020; Pang et al., 2020; Lee et al., 2021; Lee and Szymanski, 2021; Lee et al., 2025). The protein complexes that are predicted to rearrange were selected after stringent filtering for reproducibility (Figure 3; Table 1; Supplemental Dataset S6A) and presence/absence scoring between treatments (Supplemental Dataset S6C).

The most reliable predictions of ethylene-dependent multimerization variants were those in which proteins were reproducibly detected in both ethylene-treated and control samples, and the apparent mass differences were significant at 1 % FDR. These SEC elution profiles were manually inspected to ensure there was no experimental evidence pointing to the existence of the alternative form in the counter sample (Table 1). There were 13 instances in which ethylene treatment led to the complete conversion of the soluble protein to a unique higher mass complex(es) not observed in the control (class A) or the incomplete conversion of a lower mass form in the control to a higher apparent mass species (class IA). These proteins included many proteins with known functions in translation, protein stability, RNA biology, and vesicle trafficking and are strong candidates to mediate ethylene-dependent growth modulation. As one example, THO6/DWD (AT2G19430.1) appears to be a dual function protein. It is a subunit of the Arabidopsis THO/TREX mRNA export complex, which is thought to facilitate the transport of mRNA precursors and the biosynthesis of endogenous small interfering RNAs in Arabidopsis (Yelina et al., 2010). THO6/DWD is also a substrate receptor of a CUL4-based E3 ubiquitin ligase targeting ABI5, and the mutant has been reported to be ABA hypersensitive (Lee et al., 2008; Lee et al., 2010). Based on the SEC profiles, we hypothesize that ethylene signaling promotes the assembly of monomeric THO6/DWD into two distinct multimeric forms with some sort of functional importance. Given that ABA is not actively involved in regulating hypocotyl elongation in darkness, the reported ABA hypersensitivity of *tho6/dwd* (Lee et al., 2008; Lee et al., 2010) may not directly account for the altered ethylene sensitivity we observed. More plausibly, DWA1 may have additional ABA-independent roles in ethylene signaling such as mRNA export or sRNA biogenesis, affecting the stability or translation of ethylene signaling transcripts. Ethylene might play a role in this process by modulating the multimerization status of THO6/DWD, potentially directing its incorporation into distinct protein complexes that function outside of ABA signaling.

Multimerization variability in conserved vesicle trafficking and proteolytic machineries. Of note, the TOM-like 2 ubiquitin receptor (TOM2; AT1G06210.1) binds to ubiquitinated auxin efflux carrier PIN2 in affects its trafficking and turnover in the lytic vacuole (Korbei et al., 2013). Mutation of TOM2 and other orthologs leads to ABA-hypersensitivity that is correlated with increased levels of the soluble ABA receptor, and its failure to traffic to the lytic vacuole (Mazorra-Manzano et al., 2010; Moulinier-Anzola et al., 2024). In our system, ethylene treatment promotes the assembly of a novel high apparent

mass vacuolar aspartic proteinase A1 (APA1) protein complex (Shimaoka et al., 2004). The APA1 complexes in our S200 fraction likely originated from broken vacuoles, and we hypothesize that higher mass APA1 complexes reflect accelerated turnover of proteins trafficked to the vacuole (perhaps through TOM2-dependent trafficking). The mild ethylene insensitivity of *apa1* seedlings (Figure 4F), could reflect gene functions in the context of ABA signaling (Sebastian et al., 2020).

Decreased axial elongation has been correlated with observed ethylene-dependent reorientation of transverse cortical microtubule arrays and WAVE-DAMPENED2-LIKE proteins in the growth response of etiolated hypocotyls in many species, including Arabidopsis (Le et al., 2005; Sun et al., 2015). The tubulin-folding cofactor (TFC; AT2G30410.2) chaperone complex mediates α- and ß-tubulin heterodimer formation (Szymanski, 2002) and has been detected in leaves as R_{app} of ~2.0 (Aryal et al., 2017; McBride et al., 2019; Lee and Szymanski, 2021). In etiolated hypocotyls, TFC-A assembles into a distinct higher mass complex that could alter chaperone activity and either the amount of tubulin heterodimers or the particular α- and ß-tubulin isoforms that are involved in microtubule responses to ethylene. We also detected protein complex rearrangements that are predicted to affect cell wall matrix properties. UDP-glucose dehydrogenase 1 (UGD1 at first mention; AT1G26570.1) generates UDP-glucuronic acid, an essential precursor for arabinose, xylose, galacturonic acid, and apiose sugars in a variety of matrix polysaccharides are required to assemble fully functional cell walls (Reboul et al., 2011). UGD1 is the only UDP-glucose dehydrogenase detected in our dataset with no significant change in abundance (Supplemental Datasets S2 and S3), and expected to be active as a monomer (Campbell et al., 1997). Cell wall synthesis must persist to support radial expansion and shape change, it remains to be determined if the different UGD1 multimerization states affect activity and wall material properties in response to ethylene treatment.

There were also 11 examples in which ethylene promoted the disassembly or rearrangement of a protein into forms with a reduced apparent mass (Qiao et al., 2012; Wen et al., 2012). For the chaperones TCP-1 (AT3G02530.1) and calnexin (AT5G61790.1), as well as the proteasome regulatory particle 6A (AT5G19990.1), protein disassembly likely reflects a reduced activity and a fine-tuning of the cellular machineries that broadly influence the composition of the proteome. In ethylene signaling, protein complex remodeling and proteasome function are essential for rapid hypocotyl growth modulation. In the absence of ethylene, the receptor-CTR1 complex at the ER remains intact, keeping the signaling repressed (Ju et al., 2012). Upon ethylene perception, the complex disassembles, releasing EIN2, which activates the downstream ethylene signaling (Qiao et al., 2012; Wen et al., 2012). Simultaneously, ethylene promotes the degradation of EBF1/2, EIN3-targeting F-box proteins, leading to stabilization of EIN3, a key transcription factor required for ethylene-regulated growth responses (Guo and Ecker, 2003; Li et al., 2015; Merchante et al., 2015). The proteasome activity plays an integral role in these processes by regulating the turnover of key signaling components like EIN3 and EBF1/2, thus ensuring that ethylene response is quickly adjusted. Several recent studies also suggest that the proteasome itself may be dynamically regulated by post-translational modification, affecting its assembly and function (Kikuchi et al., 2010; Cui et al., 2014; Hirano et al., 2016; Marshall and Vierstra, 2019). This paper identifies dozens of additional proteins and protein complexes that are predicted to be targets of ethylene signaling.

ABCB5 is an interesting example, as it was reproducibly detected solely in the S200 fraction of ethylene-treated plants. Given the presence of multiple membrane spanning segments in the predicted structure of ABCB5 and the location of the peptides in the soluble domains, it is likely that these protein fragments are released by proteolysis (Figure 4D and 4E). The NBD2 domain mediates regulatory interaction with *cis-trans* peptidylprolyl isomerase Twisted Dwarf1 (Hao et al., 2020). It remains to be

determined if the proteolytic release of NBD2 is of regulatory importance. We failed to observe a clear growth phenotype in seedlings that overexpressed soluble NBD1 or NBD2 domains, so the protein fragment does not appear to be sufficient to alter plant development. ABCB5 somehow limits hypocotyl elongation in the absence of ethylene and consistently showed the similar reduction trends as WT in response to various ACC concentrations (Figure 4F and Supplemental figure S5), suggesting that ABCB5 is not likely involved in ethylene-regulated hypocotyl growth regulation. ABCB transporters have diverse hormone transport functions during plant development (Hu et al., 2025), and the precise role of ABCB5 remains to be determined.

Conclusions and Future Perspectives

This paper describes a new quantitative proteomics pipeline and includes useful databases on the rapid systems-level responses of the etiolated hypocotyl proteome to ethylene. Reduced protein abundance appears to be focused on the soluble proteins, and may reflect a down-regulation of cellular machineries associated with rapid axial elongation. We also detected diverse types of multimerization variants that depict an active response that includes known and predicted ATPases, proteases, carbon flux into non-cellulosic polysaccharides (Reboul et al., 2011; Vaddepalli et al., 2017), vesicle trafficking, and cytoskeletal control. We predict that these multimerization variants reflect key points of developmental control in which post-translational modifications, altered subcellular localization, or proteolytic processing facilitate specific changes in protein-protein interactions and dramatic changes in growth habit. Further analyses are needed to further validate their functional importance and determine how they operate in the context of ethylene signal transduction and developmental control.

Material and Methods

Plant materials and growth conditions

Arabidopsis Columbia (Col-0) and the ethylene-insensitive mutant, ein2-5, were used in this study (Alonso et al., 1999). All plants were sterilized and subsequently planted on the half-strengthen Murashige and Skoog (MS) media supplemented with 1 % sucrose and 0.8 % plant agar (pH 5.7). Following stratification and light activation, the plates were placed vertically positioned under a continuous dark chamber at 22°C for 3 days.

T-DNA insertion mutants, *apa1* (SALK_041027), *dwa1* (SALK_051022), and *abcb5* (CS1007014), were obtained from the Arabidopsis Biological Resource Center, and the ethylene signaling mutants, ctr1-2 (Kieber et al., 1993) and ein2-5 (Alonso et al., 1999), were used as a control.

Ethylene treatment of etiolated seedlings

The etiolated seedlings were vertically placed in a modular incubator chamber (Billups-Rothenberg) for exogenous ethylene treatment in the dark. Ethylene gas (100 ppm) was introduced into the chamber with a flow rate of 20 cc/min for 5 min, after which the stopper was closed to maintain the ethylene-treated condition for 2 hours. Following the ethylene treatment, the root and epical hook were excised using a razor blade, and the hypocotyls were collected for RNA and protein extraction. All these procedures were conducted in a dark room illuminated with green light (GONHOM A19 Green BulbE26 9W).

Measurements of hypocotyl cell length

Etiolated hypocotyls were sampled after treatment with or without ethylene for 2 hours and stained with FM™ 4-64 dye (Invitrogen, Waltham, MA, USA) following the manufacturer's instruction. Zones were defined based on cell locations starting from the hook ankle. The longitudinal cell growth was captured using an inverted confocal microscope (Zeiss, Jena, Germany). Cells from the 4th to 6th cells from the hook were designated as Zone 1, while those from the 7th to 10th cells were designated set as Zone 2.

Isolation of soluble (S200) and membrane-associated (P200) proteins

Hypocotyls were harvested from three-day-old, etiolated seedlings under a green light lamp (GONHOM A19 Green BulbE26 9W) with an additional layer of green filter paper in a dark room. Proteins were extracted from 0.65 g of fresh hypocotyls as previously described (Aryal et al., 2014; McBride et al., 2017; McBride et al., 2019; Lee and Szymanski, 2021). In brief, the fresh tissues were ground under four volumes of a cold microsome isolation buffer (MIB) [50 mM HEPES/KOH (pH 7.5), 250 mM sorbitol, 50 mM KOAc, 2 mM $Mg(OAc)_2$, 1 mM EDTA, 1 mM EGTA, 1 mM dithiothreitol (DTT), 2 mM PMSF and 1 % (v/v) protein inhibitor cocktail (160 mg/mL benzamidine-HCl, 100 mg/mL leupeptin, 12 mg/mL phenanthroline, 0.1 mg/mL aprotinin, and 0.1 mg/mL pepstatin A)] using a Polytron homogenizer (Brinkman Instruments, New York, NY, USA) with two 10-second grinding steps, interspersed with 1-minute rests. The homogenate was filtered through 4 layers of cheesecloth pre-soaked in cold MIB and then centrifuged on an Allegra X-30R centrifuge (Beckman Coulter Life Sciences, Indianapolis, IN, USA) at 1,000 × g for 10 minutes to remove debris. The supernatant was subsequently centrifuged at 200,000 × g for 20 minutes at 4°C using a Beckman Optima Ultracentrifuge (Beckman Coulter Life Sciences, Indianapolis, IN, USA) with a TLA110 rotor. The resulting supernatant was

retained as the soluble fraction (S200) enriched in cytosolic proteins and soluble proteins released from broken chloroplasts.

To enrich a membrane-associated fraction (P200), the pellet obtained from the previous centrifugation was resuspended in cold MIB, incubated on ice for 10 minutes, and ultracentrifuged at 200,000 × g for 20 minutes at 4°C. This washing step was repeated twice. To solubilize P200 proteins, we applied a sodium cholate-based extraction method with the goal of profiling P200 protein complexes responsive to ethylene. The microsomal pellet was resuspended in 4 % cholate-containing HEPES buffer and incubated with gentle rotation for 1 hour at room temperature (Basu et al., 2008; McBride et al., 2017). Solubilized P200 proteins were enriched by ultracentrifugation at 200,000 × g for 20 minutes at 4°C.

For the comparative proteomics, three biological replicates were prepared for both S200 and P200 fractions obtained from Col-0 or *ein2-5* plants, either untreated (-C_2H_4) or treated with ethylene (+C_2H_4). Protein quantification was performed using a BCA assay kit according to the manufacturer's protocol (Thermo Fisher Scientific Inc., Waltham, MA, USA). Protein yields per milligram of fresh hypocotyl were 0.55 µg/mg and 0.50 µg/mg for S200 and P200 samples, respectively.

Size Exclusion Chromatography for Co-fractionation mass spectrometry (CFMS)

For CFMS analysis (Supplemental figure S4), approximately 400 µg of S200 proteins were obtained from about 0.65 g of etiolated Col-0 hypocotyls, either untreated ($SEC_{Untreated}$) or treated with ethylene ($SEC_{Ethylene}$), as described above. The S200 proteins were resolved over a Superdex increase 200 10/300 GL column (GE Healthcare, Chicago, IL, USA) on an AKTA FPLC system (GE Healthcare, Chicago, IL, USA). The mobile phase consisted of 50 mM HEPES-KOH (pH 7.5), 100 mM NaCl, 10 mM $MgCl_2$, 5 % glycerol, and 1 mM DTT, with a flow rate of 0.65 mL/min (Lee and Szymanski, 2021). Fractions of 500 µL were collected, totaling 24 fractions, including the first two void fractions. Proteins in each fraction were precipitated using a cold acetone method. Two biological replicates were prepared for each condition. Before sample separation, the column was calibrated using the Gel Filtration Standard Kit 1000 (MWGF1000, Sigma-Aldrich, St. Louis, MO, USA).

LC-MS/MS sample preparation

Protein samples were digested using trypsin as described previously (McBride et al., 2019). Denatured protein samples in 8 M urea were reduced with 10 mM DTT for 45 minutes at 60°C, followed by alkylation with 20 mM iodoacetamide for 45 minutes at room temperature in the dark. The urea concentration was then diluted to below 1.5 M by adding 50 mM NH_4HCO_3 before trypsin digestion. Trypsin (Sigma-Aldrich, St. Louis, MO, USA) was added at an enzyme-to-protein ratio of 1:25, and digestion was performed at 37°C overnight. The reaction was stopped by adding trifluoroacetic acid. Digested peptides were purified using C18 Micro Spin Columns (74-4601, Harvard Apparatus, Holliston, MA, USA). Peptide concentrations were measured using a BCA assay (Thermo Fisher Scientific Inc.). For comparative proteomics, 1 µg of peptides was loaded onto the LC-MS/MS system. Peptide samples ($SEC_{Untreated}$ and $SEC_{Ethylene}$) from CFMS experiments were adjusted to equal volumes. The most concentrated sample had a peptide concentration of 1 µg/µL, and 1 µL of each sample was injected into the LC-MS/MS system.

LC-MS/MS data acquisition

The S200 and P200 samples for comparative proteomics were analyzed as described previously (Lee et al., 2021). Peptide samples were analyzed using a reverse-phase LC-ESI-MS/MS system on a Dionex UltiMate 3000 RSLC nano system coupled with a Q-Exactive HF Hybrid Quadrupole-Orbitrap Mass Spectrometer (Thermo Fisher Scientific Inc., Waltham, MA, USA). Peptides were resolved over a 125-minute gradient at a flow rate of 300 nL/min. An MS survey scan was acquired in the 350–1,600 m/z range. MS/MS spectra were obtained by selecting the 20 most abundant precursor ions for sequencing using high-energy collisional dissociation (HCD) with a normalized collision energy of 27 %. A 15-second dynamic exclusion window was applied to minimize redundant sequencing of the same ion.

LC-MS/MS analysis for SEC samples was performed as described (Lee et al., 2025). Peptide samples were analyzed using a reverse-phase LC-ESI-MS/MS system on a Dionex UltiMate 3000 RSLC nano system coupled with an Orbitrap Fusion Lumos Tribrid Mass Spectrometer (Thermo Fisher Scientific Inc., Waltham, MA, USA). Peptides were first loaded onto a trap column (300 μm ID × 5 mm) packed with 5-μm, 100-Å PepMap C18 material and then separated on a reverse-phase analytical column (75 μm ID × 50 cm) packed with 2-μm, 100-Å PepMap C18 material (Thermo Fisher Scientific Inc.). Peptides were resolved at a flow rate of 200 nL/min over a 160-minute LC gradient. All data were acquired in positive ion mode in the Orbitrap mass analyzer using an HCD fragmentation scheme. The MS scan range was set to 375–1,500 m/z at a resolution of 120,000. The automatic gain control (AGC) target was set to standard, with a maximum injection time of 50 ms. A dynamic exclusion of 60 seconds and an intensity threshold of 5.0e3 were applied. MS data were acquired in data-dependent mode with a cycle time of 3 s per scan.

Peptide Identification and Quantification

Protein identification and relative abundance quantification were performed using the Andromeda search engine within MaxQuant version 1.6.14.0 (Cox et al., 2014). MS/MS spectra were searched against the *Arabidopsis thaliana* TAIR10 protein database: Athaliana_167_TAIR10.protein.fa (Lamesch et al., 2012). For comparative proteomics, MS/MS spectra search for the S200 and P200 datasets were conducted independently. The search parameters were as follows: the "match between runs" function was enabled with a maximum matching time window of 0.7 min (default setting); one percent of the protein and peptide false discovery rate (FDR) was chosen; proteins identified by a single unique peptide were selected; label-free quantification (LFQ) was chosen; all other parameters were set to default. Peptide identification and quantification details are provided in Supplemental Dataset S1, while protein information for S200 and P200 is available in Supplemental Datasets S2 and S3, respectively. For CFMS analysis, searches were conducted with all fractions from biological duplicates in a single query, as previously described (Lee et al., 2025). The same search settings were applied, except that the LFQ method was not used. Peptide and protein details for CFMS are provided in Supplemental Dataset S4.

Data filtering for protein identification in comparative proteomics (S200 and P200)

To identify differentially expressed proteins upon ethylene treatment, we applied a two-step filtering strategy to each dataset independently (Lee et al., 2025). First, for the count-based data filtering, proteins identified with MS/MS count(s) ≥ 1 in at least two out of three replicates were considered identified proteins (Supplemental Datasets S2A for S200 and S3A for P200). Among these, proteins with LFQ intensities greater than zero were classified as quantified proteins. Second, for protein intensity-based filtering, only quantified proteins with LFQ intensities greater than zero in at least two out of three replicates were retained for statistical analysis (Supplemental Datasets S2B and S3B).

Determination of protein multimerization states

We applied an optimized Gaussian fitting algorithm to deconvolve the raw elution profiles into fitted peaks (McBride et al., 2017). The fitted peak locations were then converted into protein apparent mass (Consortium) values using the SEC column calibration curve described in the SEC method section. In cases where a protein elution profile could not be fitted to a Gaussian curve, the global maximum (G_{max}) was replaced by the peak location. We selected peaks that were consistently present within a two-fraction shift between biological replicates for further analysis. A protein's multimerization state (R_{app}) was defined as the ratio of the M_{app} to the theoretical monomer mass (M_{mono}) of the protein (Liu et al., 2008; Aryal et al., 2014; Lee and Szymanski, 2021). A threshold of $R_{app} \geq 1.6$ was used to define proteins as part of a complex. Peaks with M_{app} values greater than 1,200 kDa were excluded to avoid those present in the first two void fractions from the SEC separations. Raw elution profiles along with Gaussian fitted profiles are available in Supplemental figure S6, and M_{app} and R_{app} values for reproducible proteins are provided in Supplemental Dataset S5.

Detection of variations in protein abundance and multimerization states after ethylene treatment

In the comparative proteomics analysis, two-sample *t*-tests were performed between all quantified proteins, selected by protein intensity-based filtering, in the untreated ($-C_2H_4$) and ethylene-treated ($+C_2H_4$) datasets to identify differentially expressed proteins in response to ethylene treatment. LFQ intensity values were log2-transformed, and missing values were imputed by sampling from a normal distribution (width = 0.3, shift = 1.5) using Perseus version 2.0.7.0 (Tyanova et al., 2016). Statistically significant proteins were selected with a 10 % false discovery rate (FDR) and a 4-fold change threshold using Perseus' built-in tool (see columns AS to AU and BB to BD in Supplemental Datasets S2B and S3B).

To find variants in protein multimerization, *ANOVA* and Tukey's post hoc test were performed as described previously (Lee and Szymanski, 2021). The *ANOVA* tests were run against both M_{app} and R_{app} values for proteins present in both $SEC_{Ethylene}$ and $SEC_{Untreated}$ datasets. This multiple comparison test was set at a 5 % FDR to minimize likely false positives and negatives. Tukey's post hoc test was then applied at a significance level of $p < 0.05$. Statistical results were manually verified by examining the raw elution profiles of the flagged proteins in both datasets to determine if significant differences were present, as indicated by the statistical tests (Supplemental Dataset S6). Additionally, proteins with M_{app} and R_{app} differences between treatments less than 40 % (2-SEC fraction shift) were excluded from further analysis.

To identify proteins that were "potentially degraded by ethylene" or "potentially induced or stabilized by ethylene" based on the SEC data, we identified proteins were reproducible peaks in one condition and completely absent from all column fractions from the counter sample (Figure 3I; Supplemental Dataset S6C). Unreliable proteins present in the counter sample were then classified as "Unreliable: present in its counterpart SEC sample" and annotated in column AL of Supplemental Dataset S6C. Additionally, if the putatively differentially expressed protein was present in the unfractionated S200 counter sample (Supplemental Dataset S2B), they were classified as "Unreliable: detected in the Ethylene-treated dataset" or "Unreliable: detected in the Untreated control dataset" and subsequently removed.

Expression analysis of ethylene response genes by quantitative RT-PCR

Three-day-old, etiolated seedlings were treated with/without ethylene gas for 2 hours and then harvested hypocotyls under the green light condition, as aforementioned. Total RNA was extracted using RNeasy Plant Mini Kits (Qiagen, Hilden, Germany), and 1 ug of total RNA was used to synthesize cDNA with SuperScript II reverse transcriptase (Invitrogen, Waltham, MA, USA), following the manufacturers' protocols. qRT-PCR was performed using PowerUP™ SYBR™ Green Master Mix (Applied Biosystems, Waltham, MA, USA). From the S200 dataset, 21 high-confidence protein hits were statistically selected based on their abundance (Group1; Figure 2D) and stringent count-based data filtering (Group2). Specifically, proteins were included if they were identified with MS/MS counts ≥ 1 in at least two out of three replicates and were not detected in any of the replicates from the counter sample. The selected proteins are summarized in Supplemental Dataset S2C, and the primers used for downstream validation are listed in Supplemental Table S1. Three biological replicates were analyzed, and the relative expression was normalized to *actin2* as an internal control. Statistical significance was determined using a two-tailed Student's *t*-test.

Gene ontology enrichment analysis

Gene Ontology (GO) enrichment analysis was performed using agriGO v2.0 Singular Enrichment Analysis (Tian et al., 2017). The enrichment was calculated using Fisher's exact test against the TAIR genome locus (TAIR10_2017) background. The minimum number of mapping entries was 5, and Yekutieli (FDR under dependency) was used as a multi-test adjustment method. Significantly enriched GO terms in biological process (BP), GO molecular function (MF), and GO cellular component (CC) categories were reported at 5 % FDR.

Statistical tests and data analysis

Statistical analyses were performed using R version 3.5.1 (R Core Team, 2018) on RStudio 1.1.463 (RStudio Team, 2018). Gaussian fitting was applied using MATLAB_R2021a, and data organization was done using Microsoft Excel (Office 365 for Mac).

Data and materials availability

The MS raw files have been deposited into the ProteomeXchange Consortium via PRIDE under accession codes PXD061207 for the comparative proteomics and PXD061200 for the CFMS analysis. The Gaussian fitting code described in McBride *et al*. (2017) is available at (https://github.com/dlchenstat/Gaussian-fitting).

Acknowledgments

This material is based upon work supported by the National Science Foundation under Grant No. 1951819 to D.B.S and Grant No. 2245525 to G.M.Y. Also, it is supported by a Purdue Center for Plant Biology seed grant to D.B.S and G.M.Y. We thank Dr. Uma Aryal at the Purdue Proteomics Facility for running the LC/MS samples.

Supplemental Datasets

Supplemental Dataset S1. Identified peptides and proteins in the S200 and P200 cellular fractions.

Supplemental Dataset S2. Soluble proteins (S200) and differentially expressed proteins upon ethylene treatment.

Supplemental Dataset S3. Microsome-associated proteins (P200) and differentially expressed proteins upon ethylene treatment.

Supplemental Dataset S4. Raw elution profiles of peptides and proteins in CFMS analysis.

Supplemental Dataset S5. Reproducible protein peaks in ethylene-untreated ($SEC_{Untreated}$) and -treated ($SEC_{Ethylene}$) CFMS datasets (Col-0 S200).

Supplemental Dataset S6. Protein multimerization variants affected by ethylene treatment (Col-0 S200).

Supplemental Dataset S7. Enriched GO terms of multimerization variants.

Supplemental figures

Supplemental figure S1. Proteome changes in the soluble (S200) and microsome-associated (P200) cellular fractions of Col-0 and *ein2-5* etiolated plants as a response to ethylene treatment.

Supplemental figure S2. Enzyme coverages of metabolic pathways (top 80 % most abundant proteins of Col-0 S200 untreated control).

Supplemental figure S3. Enzyme coverages of metabolic pathways (top 5 % most abundant proteins of Col-0 S200 untreated control).

Supplemental figure S4. The CFMS pipeline to analyze Arabidopsis protein multimerization responses to gaseous ethylene treatment.

Supplemental figure S5. Normalized hypocotyl length of WT and *abcb5*.

Supplemental figure S6. Raw and Gaussian fitted protein elution profiles.

Supplemental tables

Supplemental Table S1. Quantitative RT-PCR Primers.

Table 1. Multimerization variants after 2 hours of ethylene exposure.

Locus ID	Name	functional category	Class*	*M* mono (kDa)	$SEC_{Untreated}$ (R_{app})			$SEC_{Ethylene}$ (R_{app})		
					Multimer		Monomer	Multimer		Monomer
					Higher-order (Larger)	Lower-order (Smaller)		Higher-order (Larger)	Lower-order (Smaller)	
AT1G06210.1	TOM2	protein turnover/vesicle trafficking	A	42.8		3.52		13.28		
AT1G03030.1	P-loop containing ATPase	ATPase	A	34.1			0.90		3.34	
AT3G28900.1	Ribosomal protein L34e superfamily protein	translation	A	13.7	81.21	22.36		79.73		
AT4G39200.2	Ribosomal protein S25 family protein	translation	A	11.9	85.08	2.01		88.83		
AT3G52150.2	RNA-binding (RRM/RBD/RNP motifs) family protein	RNA biology	A	27.7		25.81	0.82		25.30	
AT5G18820.1	TCP-1/cpn60 chaperonin family protein	protein folding	A	61.2		12.53	0.50		12.84	
AT2G40060.1	Clathrin light chain protein	vesicle trafficking	A	28.8		2.29	0.62		2.20	
AT1G79830.3	golgin candidate 5 (GC5)	vesicle trafficking	A	108.4		5.71	0.46		6.07	
AT3G19390.1	Granulin repeat cysteine protease family protein	protein stability	IA	49.3			0.73		2.61	0.76
AT1G14540.1	Peroxidase superfamily protein	redox	IA	34.4			0.83		3.00	0.83
AT2G19430.1	THO6/DWD (DDB1-binding WD40 protein) hypersensitive to ABA 1/CUL4-RBX1-DDB1-DWA1/DWA2 E3 ubiquitin-protein ligase complex/THO6	RNA biology/protein stability	IA	40.1			0.75	17.44	4.97	0.71
AT2G30410.2	tubulin folding cofactor A (KIESEL)	cytoskeleton/protein folding	IA	12.8		2.19		6.09	2.14	
AT2G19320.1	unknown	unknown	IA	8.7		3.12		19.53	3.19	
AT3G02530.1	TCP-1/cpn60/HSP60	protein stability	D	58.9	14.30	2.32			2.35	
AT3G23830.2	glycine-rich RNA-binding protein 4 (GRBP4)	RNA biology	D	14.1		4.44	0.90			0.83
AT1G64760.1	ZERZAUST, O-Glycosyl hydrolases family 17 protein	cell wall remodeling	D	52.3		8.74	1.06			1.12
AT1G60810.1	ATP-citrate lyase A-2	metabolism	D	46.8		12.06	1.08			1.19
AT5G61790.1	calnexin 1	protein stability	D/R	60.5	19.42				1.88	
AT3G25920.1	ribosomal protein L15	translation	D/R	29.7	33.27				2.73	
AT5G19990.1	regulatory particle triple-A ATPase 6A (RPT6A)	protein stability	ID	47.2		19.91			18.87	1.56
AT1G03905.1	P-loop containing ATPase	ATPase	ID	32.4		9.00			9.28	1.45
AT1G65010.1	DUF827-containing protein	unkown function	ID	152.7		4.53			4.39	0.78
AT1G26570.1	UDP-glucose dehydrogenase 1	metabolism/cell wall remodeling	ID/R	53.0	5.28			5.11	1.77	
ATCG00750.1	ribosomal protein S11 (RPS11)	translation	ID/R	15.0	48.79			53.13	6.27	

*** Classification:**

A: complete conversion to a distinct complex not observed in the Untreated control or complete conversion to a multimeric form.

IA: two-peak profile with incomplete conversion to a higher mass form.
D: complete disassembly in the Ethylene-treated to a monomeric form or to a matching peak with the Untreated control.
ID: incomplete disassembly, a pool of an assembled state is still present.
D/R: conversion from a higher-mass form to a lower-mass form that is predicted to be multimeric, and the peak is distinct from those observed in the control sample.
ID/R: D/R but incomplete conversion to a D/R form.

A full set of the multimerization variants (at 5 % FDR) can be found in Supplemental Dataset S6B.

Figures

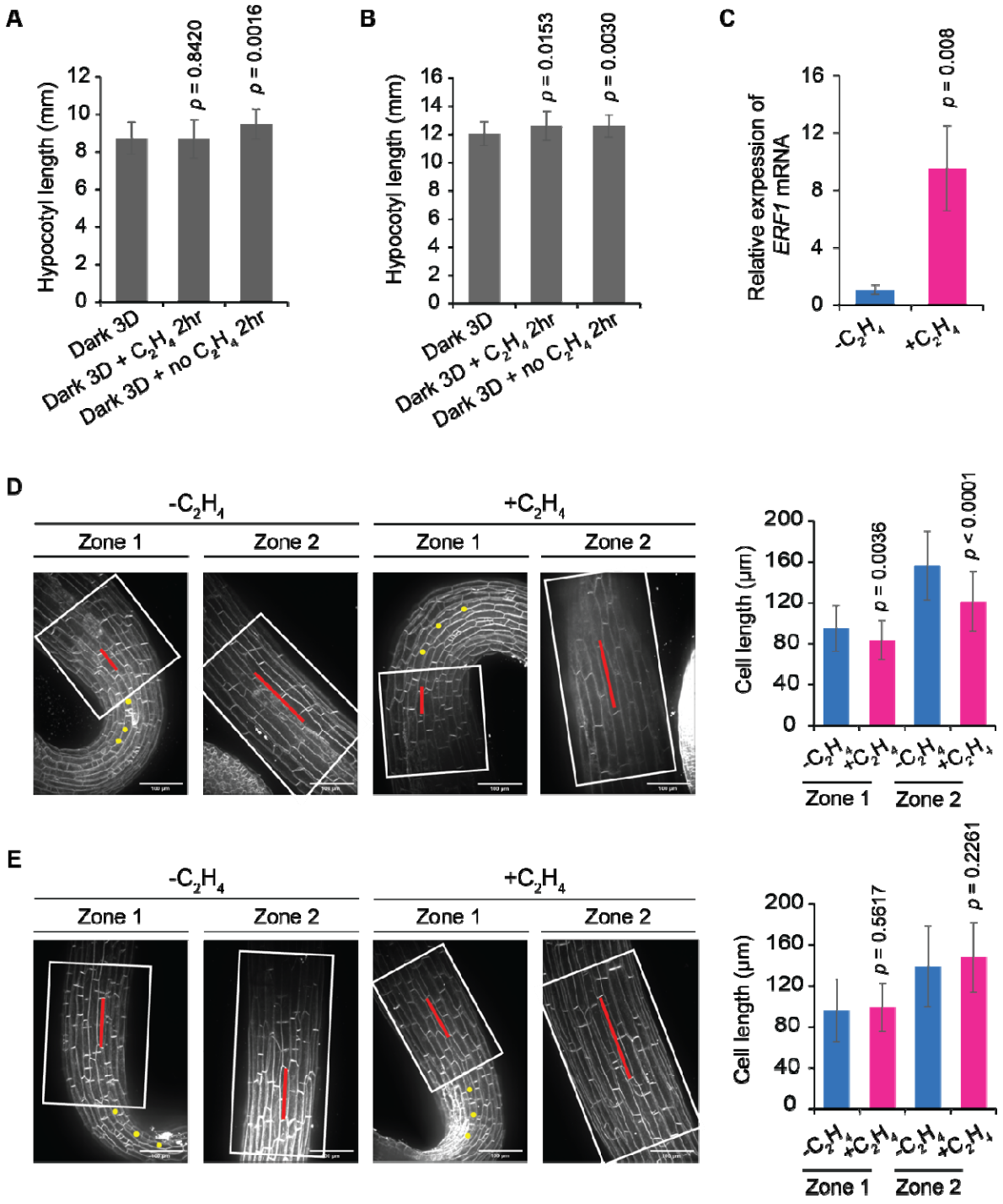

Figure 1. Ethylene treatment inhibits the growth of hypocotyl in WT but not in the *ein2-5* in the dark.

A-B, Hypocotyl length of WT (**A**) and *ein2-5* (**B**). Three-day-old, etiolated seedlings (Dark 3D) were treated with or without 100 ppm ethylene gas for 2 hours. The graphs represent the mean of hypocotyl length and the error bars, SD. Significance was determined by a two-tailed student's *t*-test to compare the hypocotyl length of seedlings with or without ethylene relative to Dark 3D.

C, Quantitative gene expression analysis of ethylene response *ERF1* without or with ethylene treatment (100 ppm). Gene expression was normalized to an Actin control and presented relative to without ethylene treatment. The error bar is SD (n = 3 biological replicates). Two-tailed Student's *t*-test.

D-E, Representative images for etiolated hypocotyls of WT (**D**) and *ein2-5* (**E**). The cell lengths of 4th-6th (zone 1) and 7th-9th (zone 2) cells from the apical hook were measured. The scale bars, 100 µm. The graph represents the average cell length of hypocotyls of WT and *ein2-5* after two hours with and without ethylene treatment. Yellow dots indicated the cells from the apical hook. Significance was determined by a two-tailed student's t-test, comparing the cell length of ethylene-treated to no ethylene-treated hypocotyls. The error bar is SD.

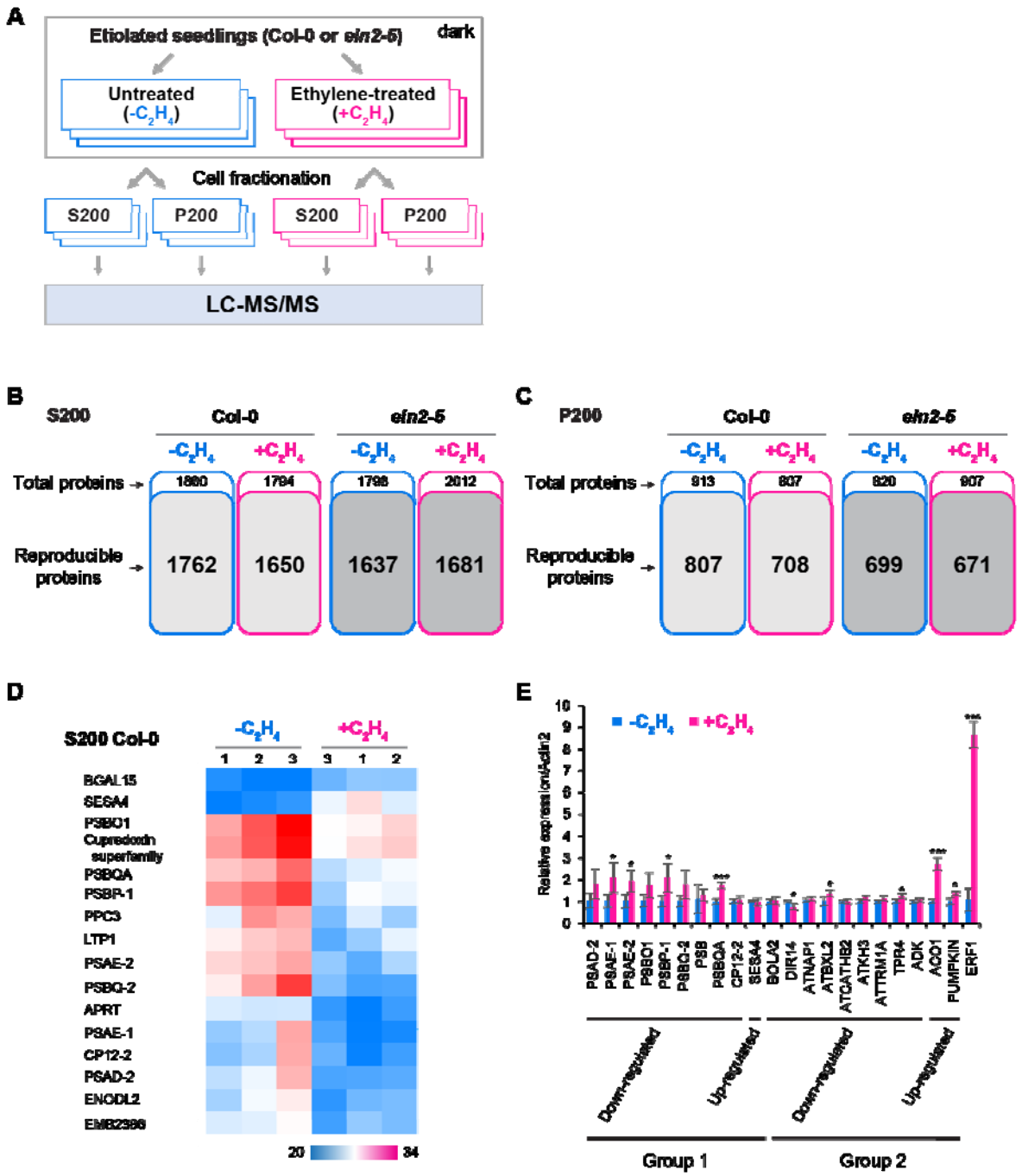

Figure 2. Quantified proteomes responding to the exogenous ethylene treatment.

A, A workflow of comparative proteomics for elucidating the effects of ethylene on the distribution of proteins in different cellular fractions. The soluble (S200) and microsome-associated (P200) proteins were extracted from three-day-old, etiolated Col-0 and *ein2-5* hypocotyls treated with (+C_2H_4) or without (-C_2H_4) gaseous ethylene. Three independent samples were prepared for LC-MS/MS analysis.

B & C, Proteome coverages of S200 (B) and P200 (C). Total proteins were defined as those identified in at least two out of three replicates. Reproducible proteins were defined as those quantified in at least two out of three replicates. The reproducible proteins in the bold text were used in the downstream analysis.

D, A heatmap of Col-0 S200 proteins differentially responding to ethylene treatment, as determined by two-sample *t*-tests at 10 % FDR with a 4-fold change threshold.

BGAL15: AT1G31740.1, SESA4: AT4G27170.1, PSBO1: AT5G66570.1, Cupredoxin superfamily AT1G20340.1, PSBQA: AT4G21280.1, PSBP-1: AT1G06680.1, PPC3: AT3G14940.1, LTP1: AT2G38540.1, PSAE-2: AT2G20260.1, PSBQ-2: AT4G05180.1, APRT: AT4G22570.1, PSAE-1: AT4G28750.1, CP12-2: AT3G62410.1, PSAD-2: AT1G03130.1, ENODL2: AT4G27520.1, EMB2386: AT1G02780.1.

E, Relative expression of S200 proteins in Col-0 in response to ethylene treatment. Three-day-old dark seedlings were treated with 100 ppm ethylene gas for 2 hours at room temperature in the dark prior to analysis. Gene expression was normalized to *Actin* control and presented relative to untreated control. Expression of the ethylene-responsive gene *ERF1* was used as a positive control to confirm the effectiveness of ethylene treatment. Error bars represent standard deviation (SD) from three biological replicates (n = 3). Group1: differentially expressed proteins detected by statistics, Group2: differentially expressed proteins identified by count-based data filtering.

BOLA2: AT5G09830.1, DIR14: AT4G11210.1), ATNAP1: AT4G26110.1, ATBXL2: AT1G02640.1, ATCATHB2: AT1G02305.1, ATKH3: AT1G33680.1, ATTRM1A: AT3G02320.1, TPR4: AT1G04530.1, ADK: AT2G37250.1, ACO1: AT2G19590.1, PUMPKIN: AT3G18680.1, ERF1: AT3G23240.1.

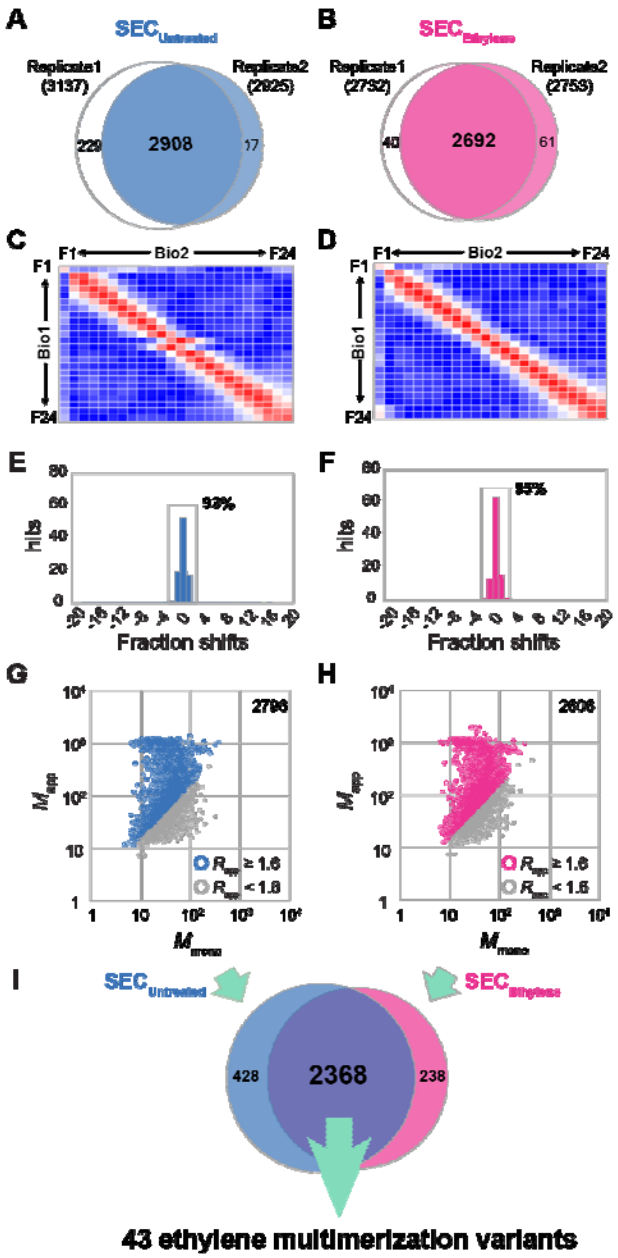

Figure 3. The CFMS pipeline allows analysis of protein multimerization responding to ethylene treatment.

A–F, Reproducibility of the CFMS datasets. Protein overlaps between two biological replicates in the untreated control (A; $SEC_{Untreated}$) and ethylene-treated (B; $SEC_{Ethylene}$) datasets obtained from S200 fraction in Col-0 plants. Pearson correlation coefficients of protein abundances across fractions in the $SEC_{Untreated}$ (C) and $SEC_{Ethylene}$ (D). Column fraction shifts between the duplicates for all proteins in the $SEC_{Untreated}$ (E) and $SEC_{Ethylene}$ (F). Reproducible proteins present within a 2-fraction shift are boxed, with the ratio of reproducibility shown.

G–H, Scatter plots of the M_{mono} and M_{app} of the reproducible proteins in the $SEC_{Untreated}$ (G) and $SEC_{Ethylene}$ (H). Open circles in grey are proteins with $R_{app} < 1.6$, while those in blue and pink have $R_{app} \geq 1.6$.

I, The test for ethylene multimerization variants. Numbers on the Venn diagram show reproducible proteins in the $SEC_{Untreated}$ and $SEC_{Ethylene}$.

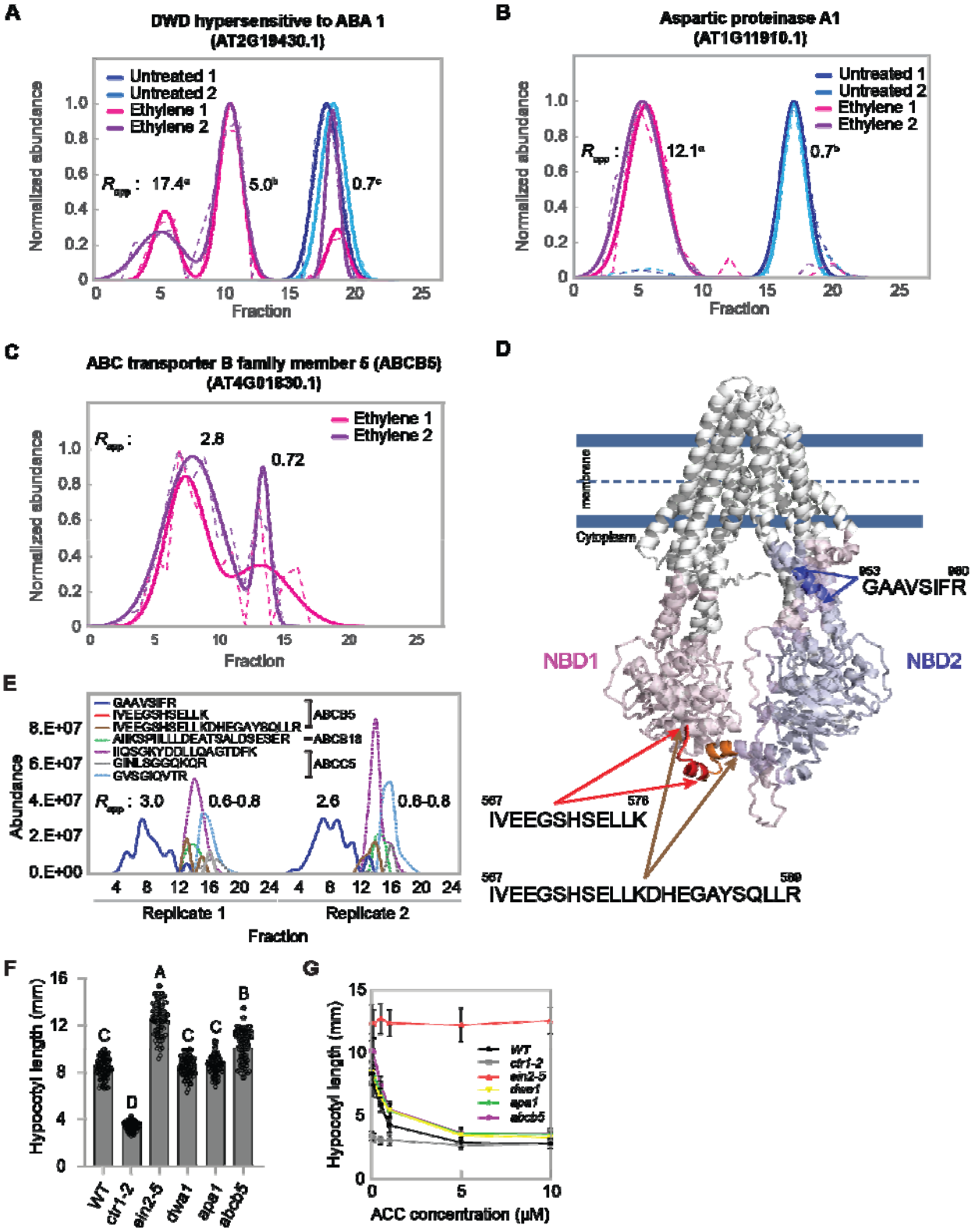

Figure 4. Protein multimerization variants in response to ethylene treatment.

A & B, Elution profiles of proteins showing ethylene-dependent changes in multimerization states.

C, Elution profiles of a protein exhibiting a putative ethylene-induced change in apparent localization.

Elution profiles of proteins in $SEC_{Untreated}$ (untreated control; blue and light blue) and $SEC_{Ethylene}$ (ethylene-treated; pink and purple) datasets were visualized across two biological replicates. Dashed lines represent raw elution profiles, while solid lines indicate Gaussian-fitted profiles. R_{app} values are shown alongside each SEC peak, with statistical groupings used to highlight significant differences in protein multimerization states following 2 hours of ethylene treatment.

D, Predicted molecular architecture of Arabidopsis ABCB5. The structural model of ABCB5 (Q9SYI3) was obtained from the AlphaFold Protein Structure Database (version updated November 2022) and visualized with the membrane. Three digested peptides identified in ethylene-treated hypocotyls are highlighted with their corresponding peptide sequences. Numbers above amino acid residues indicate their positions within the full-length ABCB5 protein sequence. NBD: nucleotide-binding domains.

E, Peptide elution profiles of three ABC transporter proteins identified after ethylene treatment. Peptides derived from the same ABC transporter proteins are grouped using blankets. Peptide elution profiles were obtained from the $SEC_{Ethylene}$ and reflect the multimerization states of the individual transporters. ABCB5: AT4G01830.1, ABCB18: AT3G28390.1, ABCC5: AT1G04120.

F, The graph shows the quantification of hypocotyl lengths of seedlings grown on MS medium without ACC for 3 days. Statistical significance was determined using one-way *ANOVA* followed by Dunnett's multiple comparisons test against the WT controls. Error bars, SD ($n \geq 70$ seedlings).

G, ACC dose-response curves for hypocotyl length of *dwa1*, *apa1*, and *abcb5* T-DNA mutant seedlings. Seedlings were grown in the media with different ACC concentrations indicated. *ctr1-2* and *ein2-5* were included as ethylene response controls. Error bars, SE ($n \geq 68$ seedlings for each ACC concentration). One-way *ANOVA* with Dunnett's test was performed to determine statistical significance.

References

Abeles FB, Morgan PW, Saltveit ME (1992) Ethylene in plant biology, Ed 2nd. Academic Press, San Diego

Achard P, Vriezen WH, Van Der Straeten D, Harberd NP (2003) Ethylene regulates arabidopsis development via the modulation of DELLA protein growth repressor function. Plant Cell **15:** 2816-2825

Aebersold R, Mann M (2016) Mass-spectrometric exploration of proteome structure and function. Nature **537:** 347-355

Ahn YO, Zheng M, Bevan DR, Esen A, Shiu S-H, Benson J, Peng H-P, Miller JT, Cheng C-L, Poulton JE, Shih M-C (2007) Functional genomic analysis of Arabidopsis thaliana glycoside hydrolase family 35. Phytochemistry **68:** 1510-1520

Alonso JM, Ecker JR (2001) The ethylene pathway: a paradigm for plant hormone signaling and interaction. Sci STKE **2001:** re1

Alonso JM, Hirayama T, Roman G, Nourizadeh S, Ecker JR (1999) EIN2, a Bifunctional Transducer of Ethylene and Stress Responses in Arabidopsis. Science **284:** 2148-2152

Andersen JS, Wilkinson CJ, Mayor T, Mortensen P, Nigg EA, Mann M (2003) Proteomic characterization of the human centrosome by protein correlation profiling. Nature **426:** 570-574

Aryal UK, McBride Z, Chen D, Xie J, Szymanski DB (2017) Analysis of protein complexes in *Arabidopsis* leaves using size exclusion chromatography and label-free protein correlation profiling. Journal of Proteomics **166:** 8-18

Aryal UK, Xiong Y, McBride Z, Kihara D, Xie J, Hall MC, Szymanski DB (2014) A proteomic strategy for global analysis of plant protein complexes. The Plant Cell **26:** 3867

Basu D, Le J, Zakharova T, Mallery EL, Szymanski DB (2008) A SPIKE1 signaling complex controls actin-dependent cell morphogenesis through the heteromeric WAVE and ARP2/3 complexes. Proceedings of the National Academy of Sciences **105:** 4044

Bellegarde F, Maghiaoui A, Boucherez J, Krouk G, Lejay L, Bach L, Gojon A, Martin A (2019) The Chromatin Factor HNI9 and ELONGATED HYPOCOTYL5 Maintain ROS Homeostasis under High Nitrogen Provision. Plant Physiology **180:** 582-592

Berry IJ, Widjaja M, Jarocki VM, Steele JR, Padula MP, Djordjevic SP (2021) Protein cleavage influences surface protein presentation in Mycoplasma pneumoniae. Sci Rep **11:** 6743

Binder BM (2007) Rapid Kinetic Analysis of Ethylene Growth Responses in Seedlings: New Insights into Ethylene Signal Transduction. Journal of Plant Growth Regulation **26:** 131-142

Binder BM, Mortimore LA, Stepanova AN, Ecker JR, Bleecker AB (2004) Short-term growth responses to ethylene in Arabidopsis seedlings are EIN3/EIL1 independent. Plant Physiol **136:** 2921-2927

Binder BM, O'Malley R C, Wang W, Moore JM, Parks BM, Spalding EP, Bleecker AB (2004) Arabidopsis seedling growth response and recovery to ethylene. A kinetic analysis. Plant Physiol **136:** 2913-2920

Bleecker AB, Kende H (2000) Ethylene: a gaseous signal molecule in plants. Annu Rev Cell Dev Biol **16:** 1-18

Campbell RE, Sala RF, van de Rijn I, Tanner ME (1997) Properties and Kinetic Analysis of UDP-glucose Dehydrogenase from Group A Streptococci: IRREVERSIBLE INHIBITION BY UDP-CHLOROACETOL *. Journal of Biological Chemistry **272:** 3416-3422

Chandrasekar B, van der Hoorn Renier AL (2016) Beta galactosidases in Arabidopsis and tomato–a mini review. Biochemical Society Transactions **44:** 150-158

Chen R, Binder BM, Garrett WM, Tucker ML, Chang C, Cooper B (2011) Proteomic responses in Arabidopsis thaliana seedlings treated with ethylene. Molecular BioSystems **7:** 2637-2650

Chien YC, Reyes A, Park HL, Xu SL, Yoon GM (2024) Uncovering the proximal proteome of CTR1 through TurboID-mediated proximity labeling. Proteomics **24:** e2300212

Chien YC, Yoon GM (2024) Subcellular dynamics of ethylene signaling drive plant plasticity to growth and stress: Spatiotemporal control of ethylene signaling in Arabidopsis. Bioessays **46:** e2400043

Consortium AIM (2011) Evidence for network evolution in an *Arabidopsis* interactome map. Science **333:** 601

Cox J, Hein MY, Luber CA, Paron I, Nagaraj N, Mann M (2014) Accurate proteome-wide label-free quantification by delayed normalization and maximal peptide ratio extraction, termed MaxLFQ. Molecular & cellular proteomics : MCP **13:** 2513-2526

Cui Z, Scruggs SB, Gilda JE, Ping P, Gomes AV (2014) Regulation of cardiac proteasomes by ubiquitination, SUMOylation, and beyond. J Mol Cell Cardiol **71:** 32-42

da Fonseca Paula CA, He J, Morris Edward P (2012) Molecular model of the human 26S proteasome. Molecular Cell **46:** 54-66

Das D, St Onge KR, Voesenek LA, Pierik R, Sasidharan R (2016) Ethylene- and Shade-Induced Hypocotyl Elongation Share Transcriptome Patterns and Functional Regulators. Plant Physiol **172:** 718-733

Du L, Song J, Forney C, Palmer LC, Fillmore S, Zhang Z (2016) Proteome changes in banana fruit peel tissue in response to ethylene and high-temperature treatments. Horticulture Research **3:** 16012

Eastmond PJ, Astley HM, Parsley K, Aubry S, Williams BP, Menard GN, Craddock CP, Nunes-Nesi A, Fernie AR, Hibberd JM (2015) Arabidopsis uses two gluconeogenic gateways for organic acids to fuel seedling establishment. Nature Communications **6:** 6659

Fan J, Yu L, Xu C (2019) Dual Role for Autophagy in Lipid Metabolism in Arabidopsis. The Plant Cell **31:** 1598-1613

Gendreau E, Traas J, Desnos T, Grandjean O, Caboche M, Hofte H (1997) Cellular basis of hypocotyl growth in Arabidopsis thaliana. Plant Physiol **114:** 295-305

Ghassemian M, Nambara E, Cutler S, Kawaide H, Kamiya Y, McCourt P (2000) Regulation of abscisic acid signaling by the ethylene response pathway in Arabidopsis. Plant Cell **12:** 1117-1126

Gilbert M, Schulze WX (2019) Global identification of protein complexes within the membrane proteome of Arabidopsis roots using a SEC-MS approach. Journal of Proteome Research **18:** 107-119

Gingras A-C, Gstaiger M, Raught B, Aebersold R (2007) Analysis of protein complexes using mass spectrometry. Nature Reviews Molecular Cell Biology **8:** 645-654

Goda H, Sawa S, Asami T, Fujioka S, Shimada Y, Yoshida S (2004) Comprehensive Comparison of Auxin-Regulated and Brassinosteroid-Regulated Genes in Arabidopsis. Plant Physiology **134:** 1555-1573

Gorka M, Swart C, Siemiatkowska B, Martínez-Jaime S, Skirycz A, Streb S, Graf A (2019) Protein Complex Identification and quantitative complexome by CN-PAGE. Scientific Reports **9:** 11523

Groban ES, Narayanan A, Jacobson MP (2006) Conformational changes in protein loops and helices induced by post-translational phosphorylation. PLoS Comput Biol **2:** e32

Guo H, Ecker JR (2003) Plant responses to ethylene gas are mediated by SCF(EBF1/EBF2)-dependent proteolysis of EIN3 transcription factor. Cell **115:** 667-677

Hao P, Xia J, Liu J, Di Donato M, Pakula K, Bailly A, Jasinski M, Geisler M (2020) Auxin-transporting ABC transporters are defined by a conserved D/E-P motif regulated by a prolylisomerase. J Biol Chem **295:** 13094-13105

Hirano H, Kimura Y, Kimura A (2016) Biological significance of co- and post-translational modifications of the yeast 26S proteasome. J Proteomics **134:** 37-46

Hu ZL, Wei H, Sun L, Russinova E (2025) Plant steroids on the move: mechanisms of brassinosteroid export. Trends Biochem Sci

Ju C, Yoon GM, Shemansky JM, Lin DY, Ying ZI, Chang J, Garrett WM, Kessenbrock M, Groth G, Tucker ML, Cooper B, Kieber JJ, Chang C (2012) CTR1 phosphorylates the central

regulator EIN2 to control ethylene hormone signaling from the ER membrane to the nucleus in Arabidopsis. Proc Natl Acad Sci U S A **109:** 19486-19491

Kikuchi J, Iwafune Y, Akiyama T, Okayama A, Nakamura H, Arakawa N, Kimura Y, Hirano H (2010) Co- and post-translational modifications of the 26S proteasome in yeast. Proteomics **10:** 2769-2779

Kim J, Lee H, Lee HN, Kim S-H, Shin KD, Chung T (2013) Autophagy-Related Proteins Are Required for Degradation of Peroxisomes in Arabidopsis Hypocotyls during Seedling Growth The Plant Cell **25:** 4956-4966

Kim Y, Seo C-W, Khan AL, Mun B-G, Shahzad R, Ko J-W, Yun B-W, Park S-K, Lee I-J (2018) Exo-ethylene application mitigates waterlogging stress in soybean (Glycine max L.). BMC Plant Biology **18:** 254

Klodmann J, Sunderhaus S, Nimtz M, JÄnsch L, Braun H-P (2010) Internal Architecture of Mitochondrial Complex I from Arabidopsis thaliana. The Plant Cell **22:** 797-810

Korbei B, Moulinier-Anzola J, De-Araujo L, Lucyshyn D, Retzer K, Khan MA, Luschnig C (2013) TOL Proteins Act as Gatekeepers for Vacuolar Sorting of PIN2 Plasma Membrane Protein. Current Biology **23:** 2500-2505

Kristensen AR, Gsponer J, Foster LJ (2012) A high-throughput approach for measuring temporal changes in the interactome. Nature Methods **9:** 907-909

Lamesch P, Berardini TZ, Li D, Swarbreck D, Wilks C, Sasidharan R, Muller R, Dreher K, Alexander DL, Garcia-Hernandez M, Karthikeyan AS, Lee CH, Nelson WD, Ploetz L, Singh S, Wensel A, Huala E (2012) The Arabidopsis Information Resource (TAIR): improved gene annotation and new tools. Nucleic Acids Research **40:** D1202-D1210

Le J, Vandenbussche F, De Cnodder T, Van Der Straeten D, Verbelen JP (2005) Cell elongation and microtubule behavior in the
hypocotyl:: Responses to ethylene and auxin. Journal of Plant Growth Regulation **24:** 166-178

Lee J-H, Terzaghi W, Gusmaroli G, Charron J-BF, Yoon H-J, Chen H, He YJ, Xiong Y, Deng XW (2008) Characterization of Arabidopsis and Rice DWD Proteins and Their Roles as Substrate Receptors for CUL4-RING E3 Ubiquitin Ligases. The Plant Cell **20:** 152-167

Lee J-H, Yoon H-J, Terzaghi W, Martinez C, Dai M, Li J, Byun M-O, Deng XW (2010) DWA1 and DWA2, Two Arabidopsis DWD Protein Components of CUL4-Based E3 Ligases, Act Together as Negative Regulators in ABA Signal Transduction The Plant Cell **22:** 1716-1732

Lee Y, Okita TW, Szymanski DB (2021) A co-fractionation mass spectrometry-based prediction of protein complex assemblies in the developing rice aleurone-subaleurone. The Plant Cell **33:** 2965-2980

Lee Y, Rani H, Mallery EL, Szymanski DB (2025) A cell fractionation and quantitative proteomics pipeline to enable functional analyses of cotton fiber development. The Plant Journal **121:** e17246

Lee Y, Szymanski DB (2021) Multimerization variants as potential drivers of neofunctionalization. Science Advances **7:** eabf0984

Lee Y, Yang P, Rani H, Miller G, Grover CE, Swaminathan S, Zabotina OA, Wendel JF, Xie J, Szymanski DB (2025) Proteomics-based models of gene expression and cellular control of cotton fiber development. bioRxiv**:** 2025.2002.2005.636703

Li Q, Ai G, Shen D, Zou F, Wang J, Bai T, Chen Y, Li S, Zhang M, Jing M, Dou D (2019) A Phytophthora capsici Effector Targets ACD11 Binding Partners that Regulate ROS-Mediated Defense Response in Arabidopsis. Molecular Plant **12:** 565-581

Li T, Yun Z, Zhang D, Yang C, Zhu H, Jiang Y, Duan X (2015) Proteomic analysis of differentially expressed proteins involved in ethylene-induced chilling tolerance in harvested banana fruit. Frontiers in Plant Science **6**

Li W, Ma M, Feng Y, Li H, Wang Y, Ma Y, Li M, An F, Guo H (2015) EIN2-directed translational regulation of ethylene signaling in Arabidopsis. Cell **163:** 670-683

Liang X, Wang H, Mao L, Hu Y, Dong T, Zhang Y, Wang X, Bi Y (2012) Involvement of COP1 in ethylene- and light-regulated hypocotyl elongation. Planta **236:** 1791-1802

Liu M, Zhang H, Fang X, Zhang Y, Jin C (2018) Auxin Acts Downstream of Ethylene and Nitric Oxide to Regulate Magnesium Deficiency-Induced Root Hair Development in Arabidopsis thaliana. Plant Cell Physiol **59:** 1452-1465

Liu X, Yang W-c, Gao Q, Regnier F (2008) Toward chromatographic analysis of interacting protein networks. Journal of Chromatography A **1178:** 24-32

Marshall RS, Vierstra RD (2019) Dynamic Regulation of the 26S Proteasome: From Synthesis to Degradation. Front Mol Biosci **6:** 40

Mazorra-Manzano MA, Tanaka T, Dee DR, Yada RY (2010) Structure-function characterization of the recombinant aspartic proteinase A1 from Arabidopsis thaliana. Phytochemistry **71:** 515-523

Mazorra-Manzano MA, Tanaka T, Dee DR, Yada RY (2010) Structure–function characterization of the recombinant aspartic proteinase A1 from Arabidopsis thaliana. Phytochemistry **71:** 515-523

McBride Z, Chen D, Lee Y, Aryal UK, Xie J, Szymanski DB (2019) A label-free mass spectrometry method to predict endogenous protein complex composition. Molecular & Cellular Proteomics **18:** 1588

McBride Z, Chen D, Reick C, Xie J, Szymanski DB (2017) Global analysis of membrane-associated protein oligomerization using protein correlation profiling. Molecular & Cellular Proteomics**:** mcp.000276.002017

McWhite CD, Papoulas O, Drew K, Cox RM, June V, Dong OX, Kwon T, Wan C, Salmi ML, Roux SJ, Browning KS, Chen ZJ, Ronald PC, Marcotte EM (2020) A pan-plant protein complex map reveals deep conservation and novel assemblies. Cell **181:** 460-474.e414

Merchante C, Brumos J, Yun J, Hu Q, Spencer KR, Enriquez P, Binder BM, Heber S, Stepanova AN, Alonso JM (2015) Gene-specific translation regulation mediated by the hormone-signaling molecule EIN2. Cell **163:** 684-697

Moulinier-Anzola J, Schwihla M, Lugsteiner R, Leibrock N, Feraru MI, Tkachenko I, Luschnig C, Arcalis E, Feraru E, Lozano-Juste J, Korbei B (2024) Modulation of abscisic acid signaling via endosomal TOL proteins. New Phytol **243:** 1065-1081

Nilsson T, Mann M, Aebersold R, Yates JR, Bairoch A, Bergeron JJM (2010) Mass spectrometry in high-throughput proteomics: ready for the big time. Nature Methods **7:** 681-685

Olinares PDB, Ponnala L, van Wijk KJ (2010) Megadalton Complexes in the Chloroplast Stroma of Arabidopsis thaliana Characterized by Size Exclusion Chromatography, Mass Spectrometry, and Hierarchical Clustering*. Molecular & Cellular Proteomics **9:** 1594-1615

Pang CNI, Ballouz S, Weissberger D, Thibaut LM, Hamey JJ, Gillis J, Wilkins MR, Hart-Smith G (2020) Analytical Guidelines for co-fractionation Mass Spectrometry Obtained through Global Profiling of Gold Standard Saccharomyces cerevisiae Protein Complexes. Molecular & Cellular Proteomics **19:** 1876-1895

Park HL, Seo DH, Lee HY, Bakshi A, Park C, Chien YC, Kieber JJ, Binder BM, Yoon GM (2023) Ethylene-triggered subcellular trafficking of CTR1 enhances the response to ethylene gas. Nat Commun **14:** 365

Park HL, Yoon GM (2025) From Growth to Stress: RAF-like Kinases as Integrators of Hormonal Signals in Plants. J Exp Bot

Peng J, Wang M, Wang X, Qi L, Guo C, Li H, Li C, Yan Y, Zhou Y, Terzaghi W, Li Z, Song CP, Qin F, Gong Z, Li J (2022) COP1 positively regulates ABA signaling during Arabidopsis seedling growth in darkness by mediating ABA-induced ABI5 accumulation. Plant Cell **34:** 2286-2308

Plücken H, Müller B, Grohmann D, Westhoff P, Eichacker LA (2002) The HCF136 protein is essential for assembly of the photosystem II reaction center in Arabidopsis thaliana. FEBS Letters **532:** 85-90

Prayitno J, Imin N, Rolfe BG, Mathesius U (2006) Identification of Ethylene-Mediated Protein Changes during Nodulation in Medicago truncatula Using Proteome Analysis. Journal of Proteome Research **5:** 3084-3095

Qiao H, Shen Z, Huang SS, Schmitz RJ, Urich MA, Briggs SP, Ecker JR (2012) Processing and subcellular trafficking of ER-tethered EIN2 control response to ethylene gas. Science **338:** 390-393

Qin H, He L, Huang R (2019) The Coordination of Ethylene and Other Hormones in Primary Root Development. Front Plant Sci **10:** 874

R Core Team (2018) R: A language and environment for statistical computing. *In*, Ed 3.5.1. R Foundation for Statistical Computing, Vienna, Austria

Reboul R, Geserick C, Pabst M, Frey B, Wittmann D, Lutz-Meindl U, Leonard R, Tenhaken R (2011) Down-regulation of UDP-glucuronic acid biosynthesis leads to swollen plant cell walls and severe developmental defects associated with changes in pectic polysaccharides. J Biol Chem **286:** 39982-39992

RStudio Team (2018) RStudio: Integrated development environment for R. *In*, Ed 1.1.463. RStudio, Inc., Boston, MA

Ruzicka K, Ljung K, Vanneste S, Podhorska R, Beeckman T, Friml J, Benkova E (2007) Ethylene regulates root growth through effects on auxin biosynthesis and transport-dependent auxin distribution. Plant Cell **19:** 2197-2212

Sánchez-Fernández Ro, Davies TGE, Coleman JOD, Rea PA (2001) The Arabidopsis thaliana ABC Protein Superfamily, a Complete Inventory*. Journal of Biological Chemistry **276:** 30231-30244

Schlossarek D, Zhang Y, Sokolowska EM, Fernie AR, Luzarowski M, Skirycz A (2023) Don't let go: co-fractionation mass spectrometry for untargeted mapping of protein–metabolite interactomes. The Plant Journal **113:** 904-914

Schomburg FM, Bizzell CM, Lee DJ, Zeevaart JA, Amasino RM (2003) Overexpression of a novel class of gibberellin 2-oxidases decreases gibberellin levels and creates dwarf plants. Plant Cell **15:** 151-163

Schonichen A, Webb BA, Jacobson MP, Barber DL (2013) Considering protonation as a posttranslational modification regulating protein structure and function. Annu Rev Biophys **42:** 289-314

Sebastian D, Fernando FD, Raul DG, Gabriela GM (2020) Overexpression of Arabidopsis aspartic protease APA1 gene confers drought tolerance. Plant Sci **292:** 110406

Senkler J, Senkler M, Eubel H, Hildebrandt T, Lengwenus C, Schertl P, Schwarzländer M, Wagner S, Wittig I, Braun H-P (2017) The mitochondrial complexome of Arabidopsis thaliana. The Plant Journal **89:** 1079-1092

Seo DH, Yoon GM (2019) Light-induced stabilization of ACS contributes to hypocotyl elongation during the dark-to-light transition in Arabidopsis seedlings. Plant J **98:** 898-911

Shimaoka T, Ohnishi M, Sazuka T, Mitsuhashi N, Hara-Nishimura I, Shimazaki K, Maeshima M, Yokota A, Tomizawa K, Mimura T (2004) Isolation of intact vacuoles and proteomic analysis of tonoplast from suspension-cultured cells of Arabidopsis thaliana. Plant Cell Physiol **45:** 672-683

Shin MH, Muneer S, Kim Y-H, Lee JJ, Bae DW, Kwack Y-B, Kumarihami HMPC, Kim JG (2020) Proteomic analysis reveals dynamic regulation of fruit ripening in response to exogenous ethylene in kiwifruit cultivars. Horticulture, Environment, and Biotechnology **61:** 93-114

Skinnider MA, Foster LJ (2021) Meta-analysis defines principles for the design and analysis of co-fractionation mass spectrometry experiments. Nature Methods **18:** 806-815

Smalle J, Haegman M, Kurepa J, Van Montagu M, Straeten DV (1997) Ethylene can stimulate Arabidopsis hypocotyl elongation in the light. Proc Natl Acad Sci U S A **94:** 2756-2761

Sun J, Ma Q, Mao T (2015) Ethylene Regulates the Arabidopsis Microtubule-Associated Protein WAVE-DAMPENED2-LIKE5 in Etiolated Hypocotyl Elongation. Plant Physiol **169:** 325-337

Swarup R, Perry P, Hagenbeek D, Van Der Straeten D, Beemster GT, Sandberg G, Bhalerao R, Ljung K, Bennett MJ (2007) Ethylene upregulates auxin biosynthesis in Arabidopsis seedlings to enhance inhibition of root cell elongation. Plant Cell **19:** 2186-2196

Szymanski D (2002) Tubulin folding cofactors: Half a dozen for a dimer. Current Biology **12:** R767-R769

Tian T, Liu Y, Yan H, You Q, Yi X, Du Z, Xu W, Su Z (2017) agriGO v2.0: a GO analysis toolkit for the agricultural community, 2017 update. Nucleic Acids Research **45:** W122-W129

Tyanova S, Temu T, Sinitcyn P, Carlson A, Hein MY, Geiger T, Mann M, Cox J (2016) The Perseus computational platform for comprehensive analysis of proteomics data. Nature Methods **13:** 731-740

Vaddepalli P, Fulton L, Wieland J, Wassmer K, Schaeffer M, Ranf S, Schneitz K (2017) The cell wall-localized atypical beta-1,3 glucanase ZERZAUST controls tissue morphogenesis in Arabidopsis thaliana. Development **144:** 2259-2269

Van de Poel B, Smet D, Van Der Straeten D (2015) Ethylene and Hormonal Cross Talk in Vegetative Growth and Development. Plant Physiol **169:** 61-72

Vandenbussche F, Vancompernolle B, Rieu I, Ahmad M, Phillips A, Moritz T, Hedden P, Van Der Straeten D (2007) Ethylene-induced Arabidopsis hypocotyl elongation is dependent on but not mediated by gibberellins. J Exp Bot **58:** 4269-4281

Vandenbussche F, Vaseva I, Vissenberg K, Van Der Straeten D (2012) Ethylene in vegetative development: a tale with a riddle. New Phytol **194:** 895-909

Verrier PJ, Bird D, Burla B, Dassa E, Forestier C, Geisler M, Klein M, Kolukisaoglu Ü, Lee Y, Martinoia E, Murphy A, Rea PA, Samuels L, Schulz B, Spalding EP, Yazaki K, Theodoulou FL (2008) Plant ABC proteins – a unified nomenclature and updated inventory. Trends in Plant Science **13:** 151-159

Veyel D, Kierszniowska S, Kosmacz M, Sokolowska EM, Michaelis A, Luzarowski M, Szlachetko J, Willmitzer L, Skirycz A (2017) System-wide detection of protein-small molecule complexes suggests extensive metabolite regulation in plants. Scientific Reports **7:** 42387

Vidal EA, Moyano TC, Krouk G, Katari MS, Tanurdzic M, McCombie WR, Coruzzi GM, Gutiérrez RA (2013) Integrated RNA-seq and sRNA-seq analysis identifies novel nitrate-responsive genes in Arabidopsis thaliana roots. BMC Genomics **14:** 701

Von Arnim A, Deng XW (1996) Light Control of Seedling Development. Annu Rev Plant Physiol Plant Mol Biol **47:** 215-243

Wang X, Wang D, Sun Y, Yang Q, Chang L, Wang L, Meng X, Huang Q, Jin X, Tong Z (2015) Comprehensive Proteomics Analysis of Laticifer Latex Reveals New Insights into Ethylene Stimulation of Natural Rubber Production. Scientific Reports **5:** 13778

Wen X, Zhang C, Ji Y, Zhao Q, He W, An F, Jiang L, Guo H (2012) Activation of ethylene signaling is mediated by nuclear translocation of the cleaved EIN2 carboxyl terminus. Cell Res **22:** 1613-1616

Xu C, Fan J (2022) Links between autophagy and lipid droplet dynamics. Journal of Experimental Botany **73:** 2848-2858

Yang P, Lee Y, Szymanski DB, Xie J (2024) A machine learning-based approach to identify reliable gold standards for protein complex composition prediction. bioRxiv**:** 2023.2010.2025.564023

Yelina NE, Smith LM, Jones AME, Patel K, Kelly KA, Baulcombe DC (2010) Putative Arabidopsis THO/TREX mRNA export complex is involved in transgene and endogenous siRNA biosynthesis. Proceedings of the National Academy of Sciences **107:** 13948-13953

Yoo SD, Cho Y, Sheen J (2009) Emerging connections in the ethylene signaling network. Trends Plant Sci **14:** 270-279

Yu Y, Wang J, Zhang Z, Quan R, Zhang H, Deng XW, Ma L, Huang R (2013) Ethylene promotes hypocotyl growth and HY5 degradation by enhancing the movement of COP1 to the nucleus in the light. PLoS Genet **9:** e1004025

Zanotti A, Coelho JPL, Kaylani D, Singh G, Tauber M, Hitzenberger M, Avci D, Zacharias M, Russell RB, Lemberg MK, Feige MJ (2022) The human signal peptidase complex acts as a quality control enzyme for membrane proteins. Science **378:** 996-1000

Zayed O, Hewedy OA, Abdelmoteleb A, Ali M, Youssef MS, Roumia AF, Seymour D, Yuan Z-C (2023) Nitrogen Journey in Plants: From Uptake to Metabolism, Stress Response, and Microbe Interaction. *In* Biomolecules, Vol 13

Zeng Y, Shen J, Li B, Jiang L (2018) Hormone modulates protein dynamics to regulate plant growth. Proc Natl Acad Sci U S A **115:** 3521-3523

Zhang X-l, Qi M-f, Xu T, Lu X-j, Li T-l (2015) Proteomics profiling of ethylene-induced tomato flower pedicel abscission. Journal of Proteomics **121:** 67-87

Zheng Q, Song J, Campbell-Palmer L, Thompson K, Li L, Walker B, Cui Y, Li X (2013) A proteomic investigation of apple fruit during ripening and in response to ethylene treatment. Journal of Proteomics **93:** 276-294

Zhu X, Liu L, Yang L, Ma F, Yang T, Fu J, Cui H (2025) ELONGATED HYPOCOTYL 5 promotes root growth by maintaining redox homeostasis and repressing oxidative stress response. Plant Physiology **197:** kiaf036

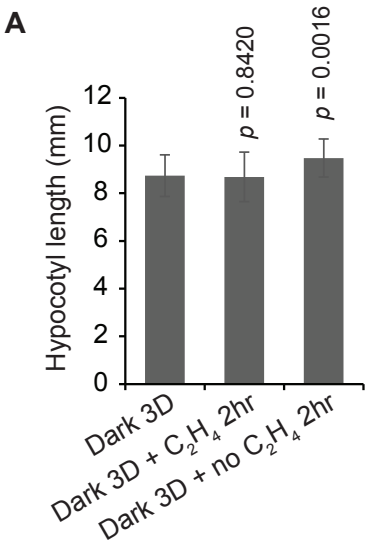
A
Hypocotyl length (mm)
0
2
4
6
8
10
12
p = 0.8420
p = 0.0016
Dark 3D
Dark 3D + C2H4 2hr
Dark 3D + no C2H4 2hr

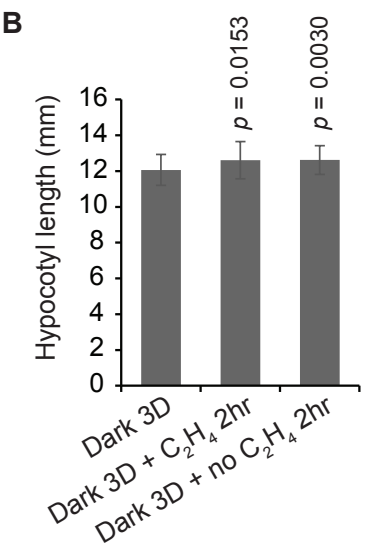
B
Hypocotyl length (mm)
0
2
4
6
8
10
12
14
16
p = 0.0153
p = 0.0030
Dark 3D
Dark 3D + C2H4 2hr
Dark 3D + no C2H4 2hr

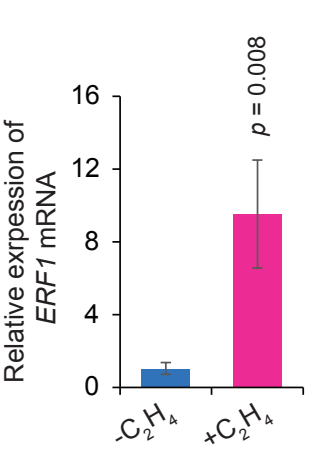
C
Relative exrpession of ERF1 mRNA
0
4
8
12
16
p = 0.008
-C2H4
+C2H4

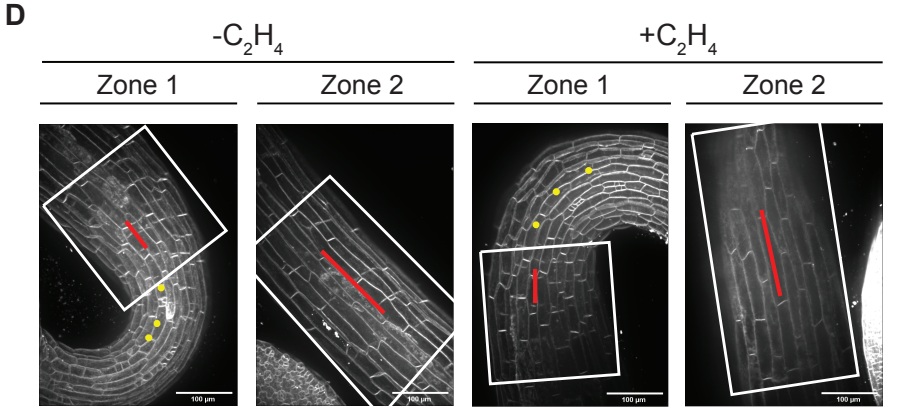
D
-C2H4
+C2H4
Zone 1
Zone 2
Zone 1
Zone 2

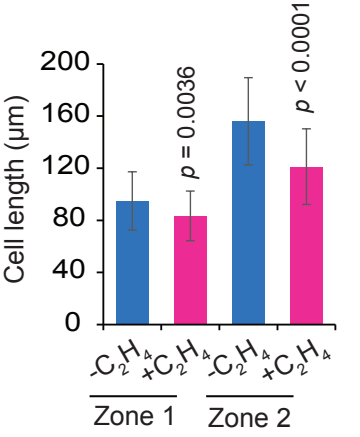
Cell length (µm)
0
40
80
120
160
200
p = 0.0036
p < 0.0001
-C2H4
+C2H4
-C2H4
+C2H4
Zone 1
Zone 2

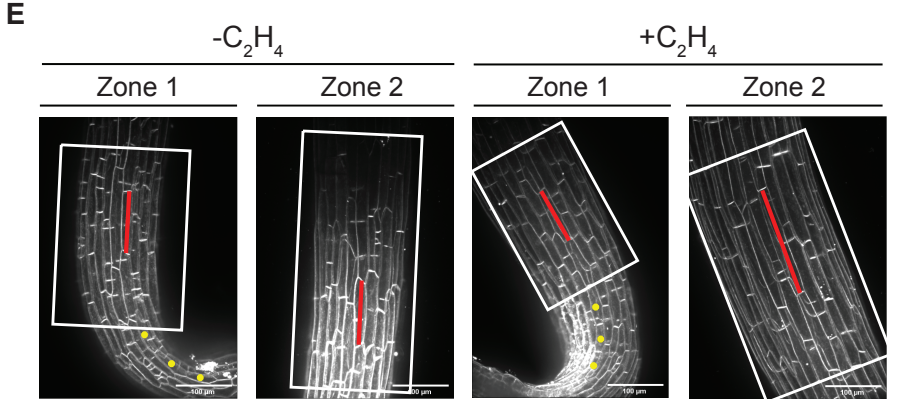
E
-C2H4
+C2H4
Zone 1
Zone 2
Zone 1
Zone 2

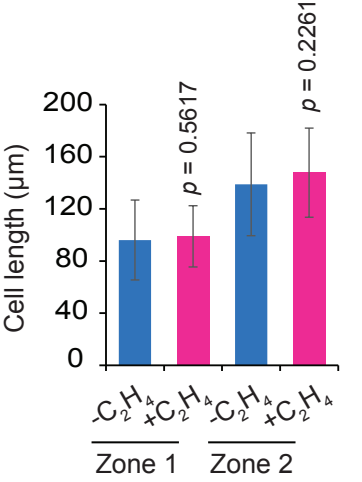
Cell length (µm)
0
40
80
120
160
200
p = 0.5617
p = 0.2261
-C2H4
+C2H4
-C2H4
+C2H4
Zone 1
Zone 2

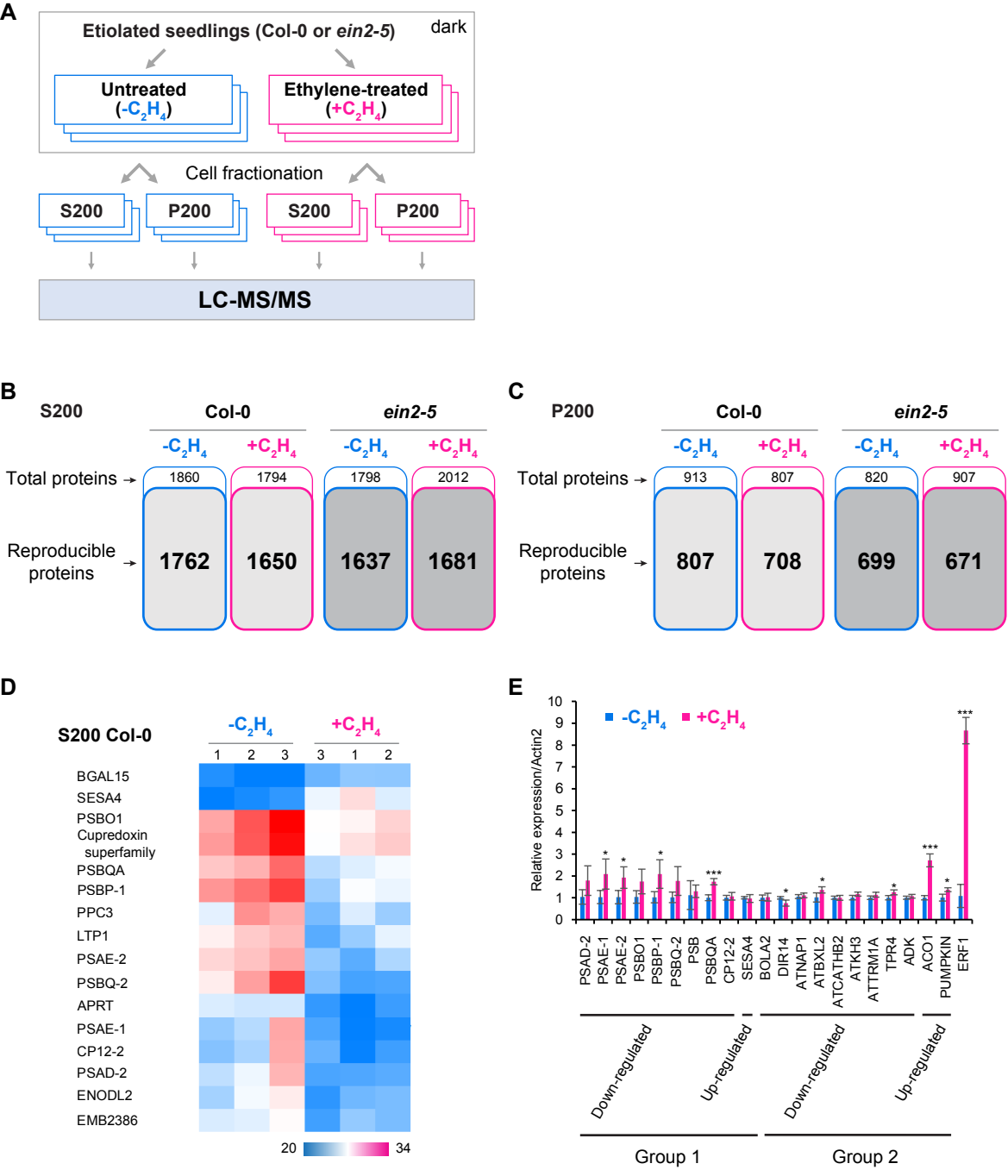
A
Etiolated seedlings (Col-0 or ein2-5)
dark
Untreated (-C2H4)
Ethylene-treated (+C2H4)
Cell fractionation
S200
P200
S200
P200
LC-MS/MS
B
S200
Col-0
ein2-5
-C2H4
+C2H4
-C2H4
+C2H4
Total proteins
1860
1794
1798
2012
Reproducible proteins
1762
1650
1637
1681
C
P200
Col-0
ein2-5
-C2H4
+C2H4
-C2H4
+C2H4
Total proteins
913
807
820
907
Reproducible proteins
807
708
699
671
D
S200 Col-0
-C2H4
+C2H4
1 2 3 3 1 2
BGAL15
SESA4
PSBO1
Cupredoxin superfamily
PSBQA
PSBP-1
PPC3
LTP1
PSAE-2
PSBQ-2
APRT
PSAE-1
CP12-2
PSAD-2
ENODL2
EMB2386
20
34
E
-C2H4
+C2H4
Relative expression/Actin2
0 1 2 3 4 5 6 7 8 9 10
PSAD-2
PSAE-1
PSAE-2
PSBO1
PSBP-1
PSBQ-2
PSB
PSBQA
CP12-2
SESA4
BOLA2
DIR14
ATNAP1
ATBXL2
ATCATHB2
ATKH3
ATTRM1A
TPR4
ADK
ACO1
PUMPKIN
ERF1
Down-regulated
Up-regulated
Down-regulated
Up-regulated
Group 1
Group 2

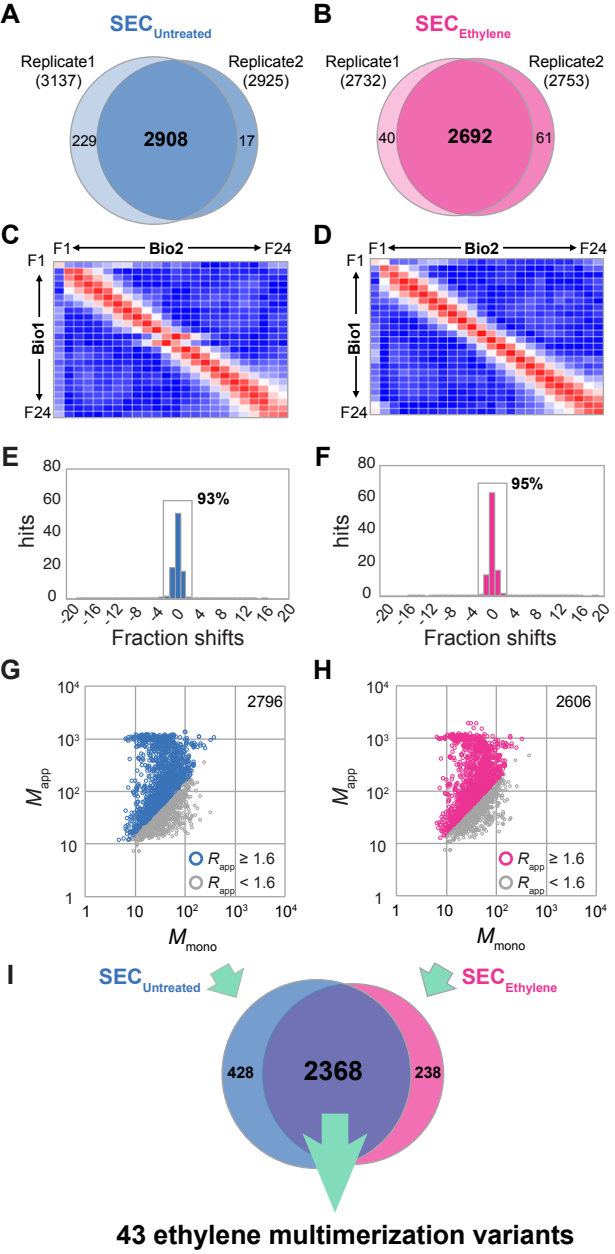
A
SEC Untreated
Replicate1 (3137)
Replicate2 (2925)
229
2908
17
B
SEC Ethylene
Replicate1 (2732)
Replicate2 (2753)
40
2692
61
C
F1
Bio2
F24
F1
Bio1
F24
D
F1
Bio2
F24
F1
Bio1
F24
E
93%
hits
Fraction shifts
F
95%
hits
Fraction shifts
G
2796
M_{app}
M_{mono}
R_{app} ≥ 1.6
R_{app} < 1.6
H
2606
M_{app}
M_{mono}
R_{app} ≥ 1.6
R_{app} < 1.6
I
SEC Untreated
SEC Ethylene
428
2368
238
43 ethylene multimerization variants

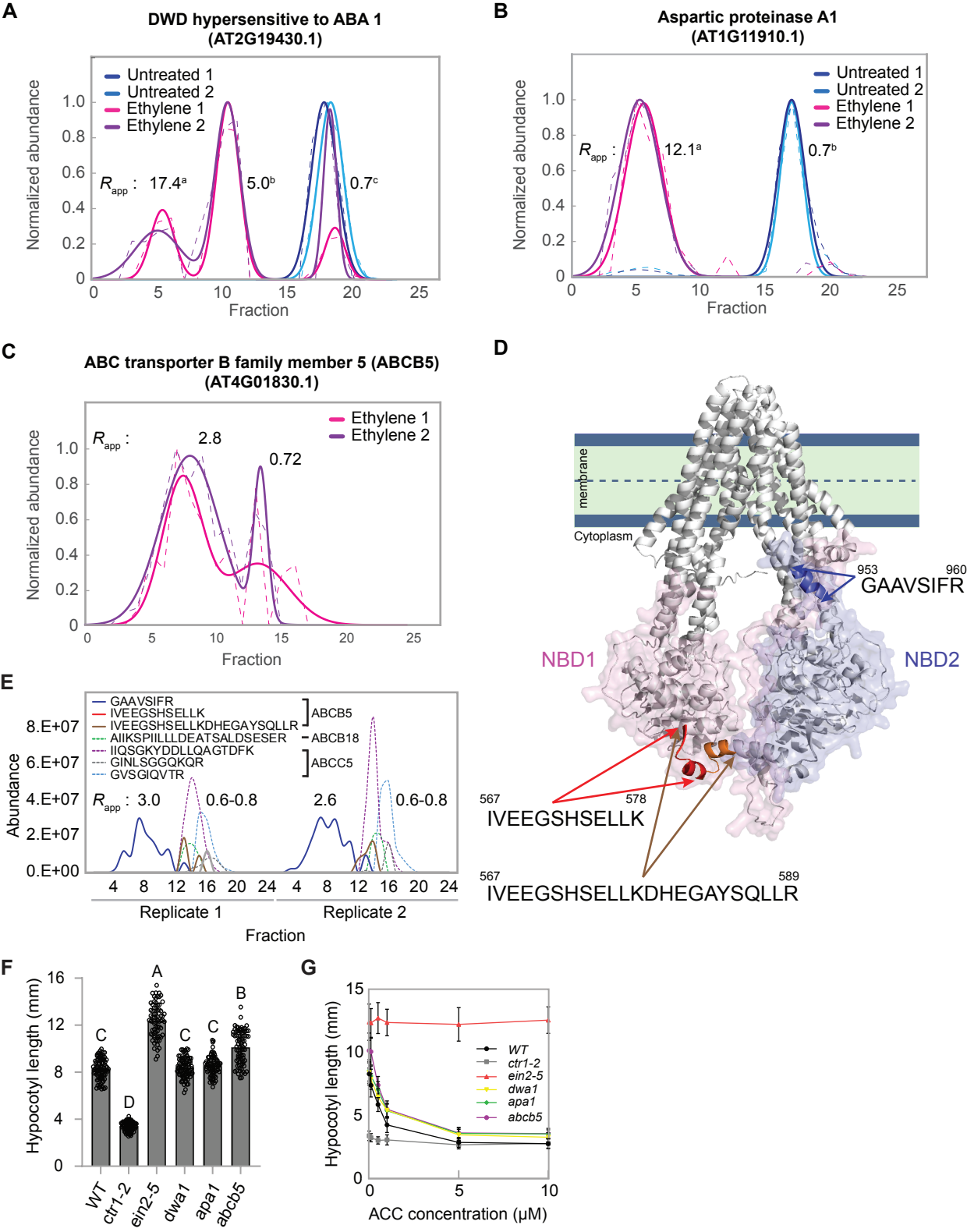
A
DWD hypersensitive to ABA 1
(AT2G19430.1)
Untreated 1
Untreated 2
Ethylene 1
Ethylene 2
Normalized abundance
R_{app} : 17.4[a]
5.0[b]
0.7[c]
Fraction
B
Aspartic proteinase A1
(AT1G11910.1)
Untreated 1
Untreated 2
Ethylene 1
Ethylene 2
R_{app} :
12.1[a]
0.7[b]
Fraction
C
ABC transporter B family member 5 (ABCB5)
(AT4G01830.1)
Ethylene 1
Ethylene 2
R_{app} :
2.8
0.72
Fraction
D
membrane
Cytoplasm
953
960
GAAVSIFR
NBD1
NBD2
567
578
IVEEGSHSELLK
567
589
IVEEGSHSELLKDHEGAYSQLLR
E
GAAVSIFR
IVEEGSHSELLK
IVEEGSHSELLKDHEGAYSQLLR
ABCB5
AIIKSPIILLLDEATSALDSESER
ABCB18
IIQSGKYDDLLQAGTDFK
GINLSGGQKQR
GVSGIQVTR
ABCC5
Abundance
R_{app} : 3.0
0.6-0.8
2.6
0.6-0.8
Replicate 1
Replicate 2
Fraction
F
Hypocotyl length (mm)
WT
ctr1-2
ein2-5
dwa1
apa1
abcb5
G
Hypocotyl length (mm)
WT
ctr1-2
ein2-5
dwa1
apa1
abcb5
ACC concentration (μM)